Novel approaches to improve estimates of short-lived halocarbon emissions during summer from the Southern Ocean using airborne observations

Elizabeth Asher[1], Rebecca S. Hornbrook[1], Britton B. Stephens[1], Doug Kinnison[1], Eric J. Morgan[5], Ralph F. Keeling[5], Elliot L. Atlas[6], Sue M. Schauffler[1], Simone Tilmes[1], Eric A. Kort[2], Martin S. Hoecker-Martínez[3], Matt C. Long[1], Jean-François Lamarque[1], Alfonso Saiz-Lopez[4,1], Kathryn McKain[7,8], Colm Sweeney[8], Alan J. Hills[1], and Eric C. Apel[1]

[1] National Center for Atmospheric Research, Boulder, Colorado, USA

[2] University of Michigan, Climate and Space Sciences and Engineering, Ann Arbor, Michigan, USA

[3] University of Redlands, Physics Department, Redlands, California, USA

[4] Department of Atmospheric Chemistry and Climate, Institute of Physical Chemistry Rocasolano, CSIC, Madrid, Spain

[5] Scripps Institution of Oceanography, University of California, San Diego, California, USA

[6] University of Miami, Department of Atmospheric Sciences, Miami, Florida, USA

[7] Cooperative Institute for Research in Environmental Sciences, University of Colorado, Boulder, Colorado, USA

[8] National Oceanic and Atmospheric Administration, Boulder, Colorado, USA

Abstract.

Fluxes of halogenated volatile organic compounds (VOCs) over the Southern Ocean remain poorly understood, and few atmospheric measurements exist to constrain modeled emissions of these compounds. We present observations of $CHBr_3$, CH_2Br_2, CH_3I, $CHClBr_2$, $CHBrCl_2$, and CH_3Br during the O_2/N_2 Ratio and CO_2 Airborne Southern Ocean (ORCAS) study and the 2nd Atmospheric Tomography mission (ATom-2), in January and February of 2016 and 2017. Good model-measurement correlations were obtained between these observations and simulations from the Community Earth System Model (CESM) atmospheric component with chemistry (CAM-Chem) for $CHBr_3$, CH_2Br_2, CH_3I, and $CHClBr_2$ but all showed significant differences in model:measurement ratios. The model:measurement comparison for CH_3Br was satisfactory and for $CHBrCl_2$ the low levels present precluded us from making a complete assessment. Thereafter, we demonstrate two novel approaches to estimate halogenated VOC fluxes; the first approach takes advantage of the robust relationships that were found between airborne observations of O_2 and $CHBr_3$, CH_2Br_2, and $CHClBr_2$; we use these linear regressions with O_2 and modeled O_2 distributions to infer a biological flux of halogenated VOCs. The second approach uses the Stochastic Time-Inverted Lagrangian Transport (STILT) particle dispersion model to explore the relationships between observed mixing ratios and the product of the upstream surface influence and sea ice, chl *a*, absorption due to detritus, and downward shortwave radiation at the surface, which in turn relate to various regional hypothesized sources of halogenated VOCs such as marine phytoplankton, phytoplankton in sea ice brines, and decomposing organic matter in surface seawater. These relationships can help evaluate the likelihood of particular halogenated VOC sources, and in the case of statistically significant correlations, such as was found for CH_3I, may be used to derive an estimated flux field. Our results are consistent with a biogenic regional source of $CHBr_3$, and both non-biological and biological sources of CH_3I over these regions.

1 Introduction

Emissions of halogenated volatile organic compounds (VOCs) influence regional atmospheric chemistry and global climate. Through the production of reactive halogen radicals at high latitudes, halogenated VOCs contribute to tropospheric and stratospheric ozone destruction, and alter the sulfur, mercury, nitrogen oxide and hydrogen oxide cycles (e.g. Schroeder et al., 1998; Boucher et al., 2003; Bloss et al., 2005; von Glasow and Crutzen; 2007; Saiz-Lopez et al., 2007; Obrist et al., 2011; Engel and Rigby, 2018). In the marine boundary layer and lower troposphere, sea salt is the main source of reactive bromine (Finlayson-Pitts 1982, Simpson et al., 2015). Yet halogenated VOCs may also be a more important source of inorganic bromine to the whole atmosphere than previously thought, according to a recent study, which indicates that sea salt is scarce and insufficient to control the bromine budget in the middle and upper troposphere (Murphy et al., 2019).

Phytoplankton and macroalgae in the ocean are the main sources to the atmosphere of several very short-lived bromocarbons, including bromoform ($CHBr_3$), dibromomethane (CH_2Br_2),

dibromochloromethane ($CHClBr_2$), and bromodichloromethane ($CHBrCl_2$) (Moore et al., 1996; Carpenter et al. 2003; Butler et al., 2007; Raimund et al., 2011). Other halogenated VOCs, such as methyl iodide (CH_3I), and methyl bromide (CH_3Br) have many natural sources, such as coastal macroalgae, phytoplankton, temperate forest soil and litter, and biomass burning (e.g., Bell et al., 2002; Sive et al., 2007; Colomb et al. 2008; Drewer et al., 2008). CH_3I is also formed through non-biological reactions in surface seawater, and CH_3Br is emitted as a result of quarantine and pre-shipment activities, which are not regulated by the Montreal Protocol (e.g., Moore and Zafiriou; 1994, Engel and Rigby, 2018). Over the Southern Ocean specifically, hypothesized sources of halogenated VOCs include: coastal macroalgae, phytoplankton, sea ice algae, and photochemical or dust stimulated non-biological production at the sea surface (e.g., Abrahamsson et al. 2018, Manley and Dastoor 1998; Moore and Zafiriou 1994; Moore et al., 1996; Richter and Wallace 2004; Williams et al., 2007; Tokarczyk and Moore 1994; Sturges et al., 1992).

We largely owe our current understanding of marine halogenated VOC emissions over the Southern Ocean to ship-based field campaigns and laboratory process studies (e.g., Abrahamsson et al. 2004a,b; Atkinson et al., 2012; Carpenter et al., 2007; Moore et al., 1996; Chuck et al., 2005; Butler et al., 2007; Raimund et al., 2011; Hughes et al., 2009; Mattsson et al. 2013; Hughes et al., 2013). These studies have reported surface water and sea-ice halogenated VOC supersaturation and corresponding elevated levels of halogenated VOCs in the marine boundary layer (MBL) in summer, and have identified numerous biological and non-biological ocean sources for these compounds. Mattsson et al. (2013) noted that the ocean also acts as a sink for halogenated VOCs, when undersaturated surface waters equilibrate with air masses transported from halogenated VOC source regions. The spatially heterogeneous ocean sources of $CHBr_3$ and CH_2Br_2 at high latitudes in the Southern Hemisphere are often underestimated in global atmospheric models (Hossaini et al., 2013; Ordoñez et al., 2012; Ziska et al., 2013). Ship-based and Lagrangian float observations provide invaluable information on the sources and temporal variability of compounds in the surface ocean. These methods offer the advantage of simultaneous measurements of both air and seawater to evaluate the gases' saturation state in the surface ocean and calculate fluxes. Yet ship-based measurements onboard these slow moving platforms also have drawbacks: they under sample the spatial variability of halogenated VOCs (e.g., Butler et al., 2007) and require assumptions about gas-exchange rates to estimate fluxes.

To disentangle the roles of atmospheric transport and spatial variability of emissions on halogenated VOC distributions requires large-scale atmospheric observations. At low latitudes, large-scale convection at the intertropical convergence zone carries bromocarbons and other halogenated VOCs into the free troposphere and lower stratosphere (e.g., Liang et al., 2014; Navarro et al., 2015). Polar regions are characterized by stable boundary layers in summer. Wind shear, frontal systems, and internal gravity waves create turbulence and control vertical mixing within and across a stable polar boundary layer (e.g. Anderson et al., 2008), and small, convective plumes may form over the marginal sea ice zone, related to sea ice leads as well as winds from ice-covered to open-ocean waters (e.g. Schnell et al., 1989). As a result of limited vertical transport in these regions, however, air-sea fluxes lead to strong vertical gradients. Zonal transport from lower latitudes has a large impact on the vertical gradients of trace gas

mixing ratios over polar regions (Salawitch 2010). Given their extended photochemical lifetimes at high latitudes (see Sect. 2.3 for a brief discussion), many halogenated VOC distributions are particularly sensitive to zonal transport at altitude.

Aircraft observations can rapidly map basin-wide vertical distributions, support quantitative flux estimates, and provide spatial constraints to atmospheric models (e.g. Xiang et al., 2010; Stephens et al., 2018; Wofsy et al., 2011). Few airborne observations of halogenated VOCs exist at high latitudes in the Southern Hemisphere. Two earlier aircraft campaigns that have measured summertime halogenated VOCs in this region are the first Aerosol Characterization Experiment (ACE-1; Bates et al., 1999) and the first High-performance Instrumented Airborne Platform for Environmental Research (HIAPER) Pole-to-Pole Observations (HIPPO; Wofsy, 2011) campaign. For these two aircraft campaigns, whole air samples were collected onboard the NSF/NCAR C-130 and the NSF/NCAR Gulfstream V (GV) during latitudinal transects over the Pacific Ocean as far south as 60° S and 67° S, respectively. However, the ACE-1 and HIPPO campaigns obtained relatively few whole air samples in this region, with ≤100 samples poleward of 60° S combined (e.g., Blake et al., 1999; Hossaini et al., 2013). ACE-1 measurements of CH_3I in the MBL indicate a strong ocean source between 40° S and 50° S in austral summer, with mixing ratios above 1.2 pmol below ~1 km (Blake et al., 1999).

Halogenated VOC emissions are frequently incorporated into earth system models, using either climatologies or parameterizations based on satellite observations of chlorophyll and geographical region and evaluated using mixing ratio comparisons with airborne observations. In Section 3.1 and 3.2, we report new airborne observations of $CHBr_3$, CH_2Br_2, CH_3I, $CHClBr_2$, $CHBrCl_2$, and CH_3Br from high latitudes in the Southern Hemisphere, where data are scarce, and large-scale regional mixing ratio comparisons for halogenated VOCs with the community earth system model (CESM) atmospheric component with chemistry (CAM-Chem). In section 3.4, we present two novel approaches to estimate regional fluxes of halogenated VOCs for comparison with global climate models' parameterizations or climatologies. One approach uses correlations of halogenated VOCs to marine, oxygen (O_2) of marine origin, as measured by deviations in the ratio of O_2 to nitrogen (N_2) ($\delta(O_2/N_2)$ see Sect. 2.1.2 and 3.1.2). We exploit robust ratios of halogenated VOCs to oxygen (O_2) determined from linear regressions (i.e. the enrichment ratio), and the ocean flux of O_2 from CESM's ocean component, to estimate the marine biogenic flux of several halogenated VOCs. The second approach relies on observed halogenated VOC mixing ratios, the Stochastic Time-Inverted Lagrangian Transport (STILT) particle dispersion model and geophysical datasets (see Sect. 2.3 and 3.3). We assess contributions from previously hypothesized regional sources for the Southern Ocean, and estimate halogenated VOC fluxes based on regressions between upstream influences and observed mixing ratios and distributions of remotely sensed data.

2 Methods

2.1 Measurements

Atmospheric measurements for this study were collected at high latitudes in the Southern Hemisphere as part of the O_2/N_2 Ratio and CO_2 Airborne Southern Ocean (ORCAS) study

(Stephens et al., 2018), and the second NASA Atmospheric Tomography Mission (ATom-2), near Punta Arenas, Chile (Fig. 1). The ORCAS field campaign took place from Jan. 15 – Feb. 29, 2016 onboard the NSF/NCAR GV. On Feb. 10 and 13, 2017 the sixth and seventh ATom-2 research flights passed over the eastern Pacific sector poleward of 60° S (defined here as Region 1) and over the Patagonian Shelf between 40° S and 55° S and between 70° W and 50° W (defined here as Region 2), respectively. The two regions for this study are defined based loosely on dynamic biogeochemical provinces identified using bathymetry, algal biomass, sea surface temperature and salinity (Reygondeau et al., 2013).

Both projects featured en route vertical profiling from near the ocean surface (~ 150 m) to the upper-troposphere, with 74 ORCAS and seven ATom-2 (during the sixth and seventh flights) low-altitude level legs in the MBL. These campaigns shared a number of instruments, including the NCAR Trace Gas Organic Analyzer (TOGA), the NCAR Atmospheric Oxygen (AO2) instrument, a Picarro cavity ringdown spectrometer operated by NOAA, discussed below. More information about individual instruments may be found in Stephens et al., 2018 and at https://www.eol.ucar.edu/field_projects/orcas and https://espo.nasa.gov/atom/content/ATom.

2.1.1 Halogenated VOCs

During ORCAS and ATom-2 TOGA provided mixing ratios of over 60 organic compounds, including halogenated VOCs. The instrument, described in Apel et al. (2015), continuously collects and analyzes samples for $CHBr_3$, CH_2Br_2, $CHClBr_2$, $CHBrCl_2$, and CH_3I among other compounds, with a 35-second sampling period and repeats the cycle every two-minutes using online fast gas chromatography and mass spectrometry. This study also leverages measurements of CH_3Br from whole air samples from the U. Miami / NCAR Advanced Whole Air Sampler (AWAS; Schauffler et al., 1999) onboard the GV during the ORCAS campaign and the UC Irvine Whole Air Sampler (WAS; Blake et al., 2001) onboard the DC-8 during the ATom-2 campaign. Halogenated VOCs reported here have an overall ±15% accuracy and ±3% relative precision, and detection limits of 0.03 ppt for CH_3I, 0.2 ppt for $CHBr_3$, 0.03 ppt for CH_2Br_2, 0.03 ppt for $CHClBr_2$, 0.05 ppt for $CHBrCl_2$, and 0.2 ppt for CH_3Br – 0.2 ppt. In addition, comparisons between onboard collected whole air samples and in-flight TOGA measurements, when sharing over half of their sampling period with TOGA measurements, showed good correlations for $CHBr_3$, CH_2Br_2, CH_3I, and $CHClBr_2$, although there were some calibration differences (Fig. S1 and Fig. S2). In addition to the comparison between co-located atmospheric measurements, we also conducted a lab inter-comparison following the campaign between NOAA's programmable flask package (PFP) and TOGA (Table S1; see supplement for details).

2.1.2 $\delta(O_2/N_2)$ and CO_2

The AO2 instrument measures variations in atmospheric O_2, which are reported as relative deviations in the oxygen to nitrogen ratio ($\delta(O_2/N_2)$), following a dilution correction for CO_2 (Keeling et al., 1998; Stephens et al., 2018). The instrument's precision is ±2 per meg units (one

in one million relative) for a 5 second measurement (Stephens et al., 2003; Stephens et al., manuscript in preparation, 2019). Anthropogenic, biogenic, and oceanic processes introduce O_2 perturbations that are superimposed on the background concentrations of O_2 in air (XO_2, in dry air = 0.2095). Air-sea O_2 fluxes are driven by both biological production and consumption of O_2 and by heating and cooling of surface waters. O_2 is consumed when fossil fuels are burned and produced and consumed during terrestrial photosynthesis and respiration. Seasonal changes in the ocean heat content lead to small changes in atmospheric N_2. As others have done, we isolated the air-sea O_2 signal by subtracting model estimates of the terrestrial O_2, fossil-fuel O_2, and air-sea N_2 flux influences from the $\delta(O_2/N_2)$ measurements (Equation 1; Keeling et al., 1998; Garcia and Keeling, 2001; Stephens et al., 2018). The difference of the $\delta(O_2/N_2)$ measurement and these modeled components is multiplied by XO_2 to convert to ppm equivalents as needed (ppm eq; Keeling et al., 1998; Equation 1).

$$O_{2\text{-ppm-equiv}} = [\delta(O_2/N_2) - \delta(O_2/N_2)_{\text{Land}} - \delta(O_2/N_2)_{\text{Fossil Fuel}} - \delta(O_2/N_2)_{N2}] \times XO_2 \quad (1)$$

We obtained the modeled $\delta(O_2/N_2)$ signal terrestrial influences from the land model component of the CESM, the fossil fuel combustion influences from the Carbon Dioxide Information Analysis Center (CDIAC; Boden et al. 2017), and the air-sea N_2 influences from the oceanic component of CESM. These fluxes were all advected through the specified dynamics version of CESM's atmosphere component, as described below in Sect. 2.2 and in Stephens et al. (2018).

CO_2 measurements were provided by NOAA's Picarro G2401-m cavity ring down spectrometer modified to have a ~1.2 sec measurement interval and a lower cell pressure of 80 Torr, which enabled the instrument to function at the full range of GV altitudes. (McKain et al. manuscript in preparation, 2019). Dry-air mole fractions were calculated using empirical corrections to account for dilution and pressure broadening effects as determined in the laboratory before and after the campaign deployments, and in-flight calibrations were used to determine an offset correction for each flight. Corrected CO_2 data have a total average uncertainty of 0.07 ppm (McKain et al. manuscript in preparation, 2019). To merge them with the TOGA data, these faster O_2 and CO_2 measurements were arithmetically averaged over TOGA's 35-s sampling periods (Stephens et al., 2017 and https://espo.nasa.gov/atom/content/ATom).

2.2 CAM-Chem model configuration

The CESM version 1, atmospheric component with chemistry (CAM-Chem) is a global three-dimensional chemistry climate model that extends from the Earth's surface to the stratopause. CAM-Chem version 1.2 includes all the physical parameterizations of Neale et al. (2013) and a finite volume dynamical core (Lin, 2004) for tracer advection. The model has a horizontal resolution of 0.9° latitude × 1.25° longitude, with 56 vertical hybrid levels and a time-step of 30 minutes. Meteorology is specified using the NASA Global Modeling and Assimilation Office (GMAO) Goddard Earth Observing System Model, version 5 (GEOS-5; Rienecker et al., 2008) (GEOS-5), following the specified dynamic procedure described by Lamarque et al. (2012). Winds, temperatures, surface pressure, surface stress, and latent and sensible heat fluxes are

nudged using a 5-hour relaxation timescale to GEOS-5 1° × 1° meteorology. The sea surface temperature boundary condition is derived from the Merged Hadley-NOAA Optimal Interpolation Sea Surface Temperature and Sea-Ice Concentration product (Hurrell et al., 2008). The model uses chemistry described by Tilmes et al. (2016), biomass burning and biogenic emissions from the Fire INventory of NCAR (FINN; Wiedinmyer et al., 2011) and MEGAN (Model of Emissions of Gasses and Aerosols from Nature) 2.1 products (Guenther et al., 2012) and additional tropospheric halogen chemistry described in Fernandez et al. (2014) and Saiz-Lopez et al. (2014). These include ocean emissions of $CHBr_3$, CH_2Br_2, $CHBr_2Cl$, and $CHBrCl_2$, with parameterized emissions based on chlorophyll *a* (chl *a*) concentrations and scaled by a factor of 2.5 over coastal regions, as opposed to open ocean regions (Ordoñez et al., 2012). The model used an existing CH_3I flux climatology (Bell et al., 2002), and CH_3Br was constrained to a surface lower boundary condition, also described by Ordoñez et al. (2012). This version of the model was run for the period of the ORCAS field campaign (January and February 2016), following a 24-month spin-up. To facilitate comparisons to ORCAS observations, output included vertical profiles of modeled constituents from the two nearest latitude and two nearest longitude model grid-points (four profiles in total) to the airborne observations at every 30-min model time-step. Following the run, simulated constituent distributions were linearly interpolated to the altitude, latitude and longitude along the flight track, yielding co-located modeled constituents and airborne observations. This version of the model has not yet been run for the ATom-2 period.

2.3 STILT model configuration

The Stochastic Time-Inverted Lagrangian Transport (STILT; Lin et al., 2003) particle dispersion model uses a receptor oriented framework to infer surface sources or sinks of trace gases from atmospheric observations collected downstream, thus simulating the upstream influences that are ultimately measured at the receptor site. The model tracks ensembles of particle trajectories backward in time and the resulting distributions of these particles can be used to define surface influence maps for each observation. STILT was run using 0.5º Global Data Assimilation System (GDAS) reanalysis winds to investigate the transport history of air sampled along the flight track (Stephens et al., 2018). For each TOGA observation, an ensemble of 4,096 particles was released from the sampling location and followed over a backwards simulation period of seven days. Particles in the lower half of the simulated MBL are assigned a surface influence value, which quantitatively links observed mixing ratios to surface sources (Lin et al., 2003). The average surface influence of all 4,096 particles per sampling location yields an hourly and spatially gridded surface influence value (ppt m^2 s $pmol^{-1}$) at a spatial resolution of 0.25º x 0.25º for each sample point.

Uncertainty in the surface influence value is strongly influenced by the accuracy of the underlying meteorological transport, as discussed in Xiang et al. (2010). We evaluated the GDAS reanalysis winds by comparing model winds interpolated in space and averaged between corresponding time points and pressure levels to match aircraft observations. By evaluating observed winds compared with modeled winds along the flight tracks we can estimate

uncertainty in the surface influence values. We consider the observation-model differences in both wind speed and direction to approximate errors in surface influence strength and location. For wind speed, a small bias may be present, where we find a median difference between observations and reanalysis of 0.68 m/s, a 5% relative bias. The 1-sigma of the wind speed difference is 2.3 m/s, corresponding to a 19% 1-sigma uncertainty in wind speed. In its simplest approximation, the surface influence strength error is perfectly correlated with the wind speed error, and thus we take 19% as an approximation of the surface influence strength uncertainty. The uncertainty in surface influence location depends on the error in the wind direction. We find a 1-sigma error of 14 degrees in wind speed, which corresponds to a possible error of 260 km/day.

Finally, we note that photochemical loss during transport is not accounted for in this analysis. Low OH mixing ratios, cold temperatures, and lower photolysis rates due to angled sunlight at high latitudes lead to longer than average halogenated VOC lifetimes. For instance, assuming an average diurnal OH concentration of 0.03 ppt, and average photochemical loss according to the Tropospheric Ultraviolet and Visible (TUV) radiation model and the Mainz Spectral data site (http://satellite.mpic.de/spectral_atlas) for Jan. 29 under clear sky conditions at 60° S, $CHBr_3$ has a lifetime of 30 days, CH_2Br_2 has a lifetime of 270 days, CH_3I has a lifetime of 7 days, and $CHClBr_2$ has a lifetime of 63 days. As such, the photochemical lifetimes of these gases are greater than or equal to the time of our back-trajectory analysis. Moreover, OH concentrations in this region have large uncertainties, the inclusion of which would lead to more, not less, uncertainty in surface influence based regression coefficients and estimated fluxes (see Sect. 2.3 and 3.3 for details).

2.3.1 STILT surface influence functions

For this study, we used STILT surface influence distributions with remotely sensed ocean surface and reanalysis data (i.e. surface source fields) in linear and multi-linear regressions to generate empirical STILT influence functions. Surface influence functions can help explain observed mixing ratios of $CHBr_3$, CH_2Br_2, CH_3Br and CH_3I, evaluate the likelihood of particular halogenated VOC sources, and in the case of statistically significant correlations, may be used to derive an estimated flux field (See Sect. 3.3 and 3.4.2 for details).

We tested whether observed mixing ratios (Z) could be explained by a linear relationship in which the predictor variable is a surface influence function, equal to the product of the surface influence (H) and a potential geophysical surface source field(s), such as chl *a*, as well as an intercept (b), a slope (a), and error term ξ (Equation 2; Fig. S5). This relationship can be generalized as a multiple linear regression with multiple surface influence functions (Hs_1, Hs_2…) and slope coefficients (a_1, a_2; Equation 3), when multiple sources contribute to observed halogenated VOC mixing ratios. The multiple linear regression may also include an interaction term (Hs_2) between predictor variables (e.g. Hs_1 and Hs_2) with a slope coefficient (a_3) to improve the fit. Statistical correlations between mixing ratios and surface influence functions may be

used to support or reject hypothesized sources. A flux (μmol m^{-2} s^{-1}) may then be estimated for each grid cell based on the product of the slopes (a_1, $a_{2...}$) and the potential source fields (s_1, $s_{2...}$). Grid cell fluxes are averaged over a geographical region to yield the average regional flux. We used the standard deviation of the regression coefficients and the relative uncertainty in the surface source, added in quadrature, to estimate the uncertainty in the flux (see Sect. 3.4.2 for fractional uncertainties). We note that the uncertainty in STILT transport (see Sect. 2.3 for details) is inherently reflected in the relative uncertainty of the regression coefficients (a_1, $a_{2...}$).

$$Z = aHs + b + \xi \quad (2)$$

$$Z = a_1 Hs_1 + a_2 Hs_2 + (a_3 Hs_1 Hs_2) \ldots + b + \xi \quad (3)$$

2.3.2 Surface Source Fields

Geophysical surface source fields of remotely sensed and reanalysis data included a combination of sea ice concentration, chl *a*, absorption due to ocean detrital material, and downward shortwave radiation at the ocean surface.

We used daily sea ice concentration data (https://nsidc.org/data/nsidc-0081) at a 25 km x 25 km spatial resolution between 39.23° S and 90° S, 180° W – 180° E from the NASA National Snow and Ice Data Center Distributed Active Archive Center (NSIDC; Maslanik et al., 1999). This data reports the fraction of sea-ice cover, land-ice cover, and open water. Unfortunately, these data do not provide any information on sea ice thickness, or the presence of brine channels or melt ponds, which may modulate emissions from sea-ice covered regions. Sea ice concentration data were calculated using measurements of near-real-time passive microwave brightness temperature from the Special Sensor Microwave Image/Sounder (SSMIS) on the Defense Meteorological Satellite Program (DMSP) satellites. NSIDC sea ice concentration data were arithmetically averaged to yield 0.25° x 0.25° binned sea ice fraction for use with gridded surface influences.

Due to persistent cloud cover over the Southern Ocean, which often precludes the retrieval of remotely sensed ocean color data, we used 8-day mean composite Aqua MODIS L3 distributions of chl *a* from the Ocean Color Index (OCI) algorithm and absorption due to gelbstoff and detrital material at 443 nm from the Generalized Inherent Optical Properties (GIOP) model (NASA Goddard Space Flight Center, 2014). Absorption due to gelbstoff and detrital material at 443 nm is used as a proxy for colored dissolved organic matter (CDOM; https://oceancolor.gsfc.nasa.gov/atbd/giop/). CDOM is hypothesized to be an important source of carbon for the photochemical production of CH_3I (Moore et al., 1994). The GIOP model also publishes an uncertainty in the absorption due to gelbstoff and detrital material at 443 nm. Raw 4 km x 4 km data were geometrically averaged, based on lognormal probability density functions, to a spatial resolution of 0.25° x 0.25° for use with gridded surface influences. We used the ratio of the 0.25° x 0.25° gridded uncertainty in the detrital material absorption to the absorption as the relative uncertainty for flux calculations (see Sect. 3.4.2).

The National Center for Environmental Prediction (NCEP) provides Final Global Data Assimilation System (GDAS/FNL) global data of downward shortwave radiation at the surface at 0.25 degree and 6-hour resolution (NCEP, 2015). We chose downward shortwave radiation for use with gridded surface influences because the photo-production of CH_3I has been observed at all visible wavelengths (Moore et al., 1994). This reanalysis data is available at a higher temporal resolution and better spatial coverage than satellite retrievals of photosynthetically active radiation (PAR) or temperature.

3 Results and discussion

3.1 Observed halogenated VOC patterns and relationships

Zonal cross-sections of halogenated VOC data collected on ORCAS and ATom-2 illustrate unprecedented spatial sampling across our study area between the surface and 12 km (Fig. 2). Above average mixing ratios of CH_3I, $CHBr_3$, and $CHClBr_2$ typically remain confined to the lower ~2-4 km of the atmosphere (Fig. 2a, b, d). These compounds have lifetimes of approximately two months or less. Conversely, weak sources and longer lifetimes (≥ 3 months) may have contributed to similar concentrations of CH_2Br_2 and $CHBrCl_2$ throughout the troposphere and above average mixing ratios as high as 8 km (Fig. 2c, e). Unfortunately, the availability of data above the detection limit and absence of BL enhancements for $CHBrCl_2$ preclude the identification of strong regional sources at this time. Meridional distributions also indicate lower latitude sources of CH_3I and CH_3Br (< 50° S), potentially resulting from terrestrial and anthropogenic contributions, and higher latitude sources (> 60° S) of $CHBr_3$, CH_2Br_2, and $CHClBr_2$ (Fig. 2a-d,f).

3.1.1 Observed halogenated VOC interrelationships

Across our study area in both 2016 and 2017, we found that $CHBr_3$ and CH_2Br_2 exhibit a consistent enhancement ratio with each other in the bottom 2 km of the atmosphere both in Region 1 and Region 2, which suggests that these bromocarbon fluxes are closely coupled. Previous studies have documented co-located source regions of $CHBr_3$ and CH_2Br_2 in the Southern Ocean (e.g. Hughes et al., 2009; Carpenter et al., 2000; Nightingale et al., 1995; Laturnus et al., 1996), and laboratory studies have demonstrated that phytoplankton and their associated bacteria cultures, including a cold water diatom isolated from coastal waters along the Antarctic Peninsula and common to the Southern Ocean, produce both $CHBr_3$ and CH_2Br_2 (Hughes et al., 2013; Tokarczyk and Moore 1994, Sturges et al., 1993). The non-linearity observed in ratios of these two gases at low $CHBr_3$ may reflect the different rates of their production or loss in seawater, or possibly, the influence of air masses from distant, more productive low-latitude source regions. Several studies have documented bacterially mediated loss of CH_2Br_2, but not $CHBr_3$, and report distinct ratios of CH_2Br_2 to $CHBr_3$ in seawater during the growth and senescent phases of a phytoplankton bloom (e.g. Carpenter et al., 2009, Hughes et al., 2013). Although this analysis is restricted to the bottom 2 km of the atmosphere, zonal

transport of air masses with lower ratios of CH_2Br_2 to $CHBr_3$ ratios, as have been observed in the MBL over productive, low-latitude regions, may also have influenced our observations (Yokouchi et al. 2005). Mixing ratios of $CHBr_3$ and $CHClBr_2$ were also correlated (Fig. 3d) in Region 2, and, a similar, weaker relationship was observed in Region 1 (Fig. 3b). $CHClBr_2$ is a less well-studied compound than CH_2Br_2. Yet these consistent relationships suggest that $CHBr_3$ and $CHClBr_2$ may either share some of the same sources or have sources that co-vary.

3.1.2 Observed halogenated VOC relationships to $\delta(O_2/N_2)$ and CO_2

We sought to test if the biologically mediated production of bromocarbons and oxygen result in similar atmospheric distributions. Conversely, we expected halogenated VOC atmospheric distributions and CO_2 distributions to anticorrelate because CO_2 fixation in surface waters is proportional to the production of oxygen.

For these comparisons, both O_2 and CO_2 mixing ratios from the upper troposphere (5-7 km) were subtracted from the data to detrend for seasonal and inter-annual variability (Fig. 4; Fig. S3). To isolate the contribution of ocean O_2 fluxes, the ORCAS $\delta(O_2/N_2)$ values reported here represent the $\Delta\delta(O_2/N_2)$ to observed values between 5-7 km adjusted for CESM O_2 land and fossil fuel contributions and the influence of air-sea N_2 fluxes. In Fig. 4 we present type II major axis regression fits to data (fits were calculated using data scaled to their full range) between the ocean surface and the lowest 7 km for bromocarbons with photochemical lifetimes of ≥ 1 month and from the lowest 2 km for CH_3I with a photochemical lifetime of ~ 1 week. We used a type II major axis regression model to balance the influences of uncorrelated processes and measurement uncertainty in halogenated VOCs (on the y-axis) and uncorrelated processes and measurement uncertainty in O_2 and CO_2 (on the x-axis) on the regression slope (Ayers et al., 2001; Glover et al., 2011). As noted by previous studies, simple least squares linear regressions fail to account for uncertainties in predictor variables (e.g. Cantrell et al., 2008).

The robust correlations of $CHBr_3$ and CH_2Br_2 with $\delta(O_2/N_2)$, in both 2016 and 2017 and in Region 1 and Region 2, provides support for a regional biogenic source of these two halogenated VOCs (Fig. 4a, b and Fig. 4d, e). The air-sea exchange of O_2 during summer in the Southern Ocean is driven by net community production (the excess of photosynthesis over respiration) in the surface mixed layer, surface warming, and to a lesser extent ocean advection and mixing (e.g. Stephens et al., 1998; Tortell and Long 2009; Tortell et al., 2014). Note that we adjust for influences on the $\delta(O_2/N_2)$ from thermal N_2 fluxes (see Equation 1, Sect. 2.1.2 for details). Biological O_2 supersaturation in the surface mixed layer develops quickly in the first several days of a phytoplankton bloom and diminishes as community respiration increases and air-sea gas exchange equilibrates the surface layer with the atmosphere on a timescale of ~ 1 week. $CHBr_3$ and CH_2Br_2 are emitted from phytoplankton during the exponential growth phase (Hughes et al., 2013), which often coincides with high net community production and the accumulation of O_2 in surface waters. The bulk air-sea equilibration time for an excess of $CHBr_3$ and other halogenated VOCs is less than two weeks, although the photochemical loss of

418 halogenated VOCs will alter their ratio over time (see Supplement for details on calculations of
419 bulk sea air equilibration times).

420 Our observations suggest a biological source for $CHBr_3$ and CH_2Br_2 in both Region 1 and Region
421 2 (Fig. 4). Interestingly, the slope of the regression between $CHBr_3$ and O_2 appears distinct in
422 Region 1 and Region 2, but between CH_2Br_2 is the same. Molar enrichment ratios are 0.20 ±
423 0.01, and 0.07 ± 0.004 pmol : mol for $CHBr_3$ and CH_2Br_2 to O_2 in Region 1, and 0.32 ± 0.02, and
424 0.07 ± 0.004 pmol : mol in Region 2. We observe a weaker relationship between CH_3I and
425 $CHClBr_2$ and O_2 in Region 1 (Fig. 4c, d), consistent with the existence of other, non-biological
426 sources of CH_3I in this region. Figure 4f illustrates a strong relationship between CH_3I and O_2,
427 as well as $CHClBr_2$ and O_2, in Region 2, however, which implies that the dominant sources of
428 CH_3I and $CHClBr_2$ emissions over the Patagonian Shelf are biological. The corresponding molar
429 enrichment ratios of CH_3I to O_2 and $CHClBr_2$ to O_2 in Region 2 are 0.38 ± 0.03 pmol : mol and
430 0.19 ± 0.04 pmol: mol, respectively.

431 In contrast to O_2, air-sea fluxes of CO_2 over the Southern Ocean during summer reflect the
432 balance of opposing thermal and biological drivers (e.g. Stephens et al., 1998; 2018). Ocean
433 buffering chemistry results in CO_2 equilibration across the air-sea interface on a timescale of
434 several months. ORCAS observations showed a depletion of CO_2 in the MBL, indicating that
435 uptake driven by net photosynthesis dominated over thermally driven outgassing during the
436 several months preceding the campaign (Stephens et al., 2018). $CHBr_3$ and CH_2Br_2 in the
437 lowest 7 km were negatively correlated with CO_2 in both years in Region 1 and Region 2 (Fig.
438 S3a, b, d, e). Interestingly, CH_3I was not correlated with CO_2 in Region 1, likely due to the long
439 air-sea equilibration timescale of CO_2 compared with a 9-day air-sea equilibration time and a ~7-
440 day photochemical lifetime for CH_3I. For longer lived species, correlations for halogenated
441 VOCs to CO_2 have similar r^2-values as those for halogenated VOCs to $\delta(O_2/N_2)$, but model and
442 climatological estimates of Southern Ocean CO_2 fluxes are much less certain than for O_2 (Anav
443 et al., 2015; Nevison et al., 2016). As a result, we use modeled O_2 fluxes as the basis for our
444 halogenated VOC flux estimates (see Sect. 3.4.1 for details).

445

446 **3.2 Model-observation comparisons**

447 The ORCAS dataset provides an exceptional opportunity to evaluate the CAM-Chem
448 halogenated VOC emission scheme (Ordoñez et al., 2012) at high latitudes in the Southern
449 Hemisphere. We compared modeled halogenated VOC constituents to corresponding
450 observations along the ORCAS flight track (Fig. 5; Fig. 6). In these figures, we used type II
451 major axis regression models to balance the measurement uncertainty (on the y-axis) and the
452 inherent, yet difficult to quantify representativeness and errors in a global atmospheric chemistry
453 model (on the x-axis). We note that this comparison may favor constituents with longer
454 photochemical lifetimes, when transport and mixing dominate over source heterogeneity.

455 In Region 1 and Region 2, both the model and observations indicate that elevated mixing ratios
456 of CH_3I remain confined to the MBL (Fig. 5a and Fig. 6a), presumably due to its relatively short

photochemical lifetime. Modeled and observed CH_3I are poorly correlated in Region 1 (r^2 = 0.20; Fig. 5b) and better correlated in Region 2 (r^2 = 0.70; Fig. 6b). In both regions, the model most likely under predicts CH_3I in the upper troposphere and lower stratosphere (UTLS), likely stemming from the poleward transport of lower latitude air masses, where CAM-Chem also exhibits a negative bias. Mixing ratio comparisons with CAM-Chem over the tropics (see Figure 10 in Ordoñez et al., 2012) depict similar or larger discrepancies, and have been attributed to stronger than anticipated convective cells in the tropics. We found strong correlations and agreement to within a factor of ~2 between modeled and observed $CHBr_3$ and CH_2Br_2 (Fig. 5c-f and Fig. 6c-f). Relatively long lifetimes (≥ 1 month) in Region 1 likely enable vertical and zonal transport of $CHBr_3$ and CH_2Br_2 to the mid and upper troposphere (Fig. 5c and e). The model was biased low with respect to measurements of CH_3Br by ~25% in Region 1 and Region 2 (Fig. 5g-h and Fig. 6g-h), potentially as a result of an incorrect surface lower boundary condition. The model underpredicted the mean vertical gradient in $CHClBr_2$, although it did a reasonable job of representing the mean vertical gradient in $CHBrCl_2$, in both Region 1 and Region 2. In both cases, however, the model failed to capture the spatial variability in both $CHClBr_2$ and $CHBrCl_2$ observations (Fig. 5i-l and Fig. 6i-l). Region 2 contains stronger sources of halogenated VOCs than Region 1, which has been documented in numerous ship-based campaigns and archived in the Halocarbons in the Ocean and Atmosphere database (HalOcAt; https://halocat.geomar.de/). Region 2 also has much higher chl *a* (Fig. S4), supporting biogenic sources for these gases.

3.3 Relationships between STILT surface influence functions and observations

We used the STILT model to explore the relationships between observed mixing ratios and the upstream surface influence functions (Equations 2-3) of sea ice, chl *a*, absorption due to detritus, and downward shortwave radiation at the surface, which relate to various regional hypothesized sources of halogenated VOCs such as marine phytoplankton, phytoplankton in sea ice brines, and decomposing organic matter in surface seawater (e.g. Moore and Zafiriou 1994; Moore et al., 1996; Tokarczyk and Moore 1994; Sturges et al., 1992).

We found no positive relationships between upstream sea-ice influence and any measured halogenated VOC Region 1 (Fig. 7). We interpret this result to mean that increased summertime sea ice acts either to reduce the production of halogenated VOCs by blocking sunlight or as a physical barrier to oceanic emissions of halogenated VOCs from under-ice algae. Both of these mechanisms are also consistent with a link between enhanced $CHBr_3$ and CH_2Br_2 emissions due to sea-ice retreat and surface sea-ice melt water (Carpenter et al., 2007).

In other studies, it has also been proposed that sea ice could be an important source for $CHBr_3$ and other halogenated VOCs, since high mixing ratios of $CHBr_3$ have been observed at the sea-ice and ice-snow interface in the austral winter (Abrahamsson et al., 2018) and in under-ice algae in the austral spring (Sturges et al., 1993). At present, CAM-Chem v1.2 with very short-lived halogen chemistry does not include a regional flux of halogenated VOCs over sea-ice covered waters in summer, and our results do not indicate a need to include one. Our data, which were

collected in January and February, however, cannot assess the importance of sea ice as a source of halogenated VOCs in other seasons, such as winter or spring (Abrahamsson et al., 2018; Sturges et al., 1993). More field campaigns are needed to further study the seasonality and regional strength of sea ice related halogenated VOC emissions.

We observed a statistically significant positive correlation between the surface influence function of 8-day satellite composites of chl *a* concentration, which is widely used as a proxy for near-surface phytoplankton biomass, and mixing ratios of $CHBr_3$ and CH_2Br_2 in Region 1 (Fig. 8a, b). This finding corroborates previous findings from ship-borne field campaigns and laboratory studies that have suggested a biogenic source for these two bromocarbons *(*e.g., Moore et al., 1996; Hughes et al., 2013*),* and further substantiates the current CAM-Chem parameterization of regional bromocarbon emissions using satellite retrievals of chl *a* in polar regions. CH_3Br mixing ratios were not significantly correlated with chl *a* surface influence functions (Fig. 8c). Although potentially suggesting that marine phytoplankton and microalgae were not a strong regional source of CH_3Br during ORCAS, it is also possible that the relatively long lifetime of CH_3Br precludes a definitive analysis of its origin based on chl *a* using 7-day back-trajectories. Neither $CHClBr_2$ nor $CHBrCl_2$ were significantly correlated with chl *a* composite surface influence functions (data not shown); however, more observations of these short-lived species in the remote MBL are needed to substantiate this result.

Similar to Lai et al. (2011), we observed a significant correlation between mixing ratios of CH_3I and total weekly upstream influence functions of 8-day chl *a* composites (Fig. 8d). Weaker correlations were observed with upstream influence functions on shorter timescales than seven days. We found that CH_3I, particularly in Region 1, was better explained by a multi-linear regression with two predictors: 1) the influence function of downward shortwave radiation at the surface (Fig. 9a) and 2) the absorption of light due to detrital material (Fig. 9b), yielding improved agreement between predicted and observed CH_3I (Fig. 9c). Several previous studies have correlated mixing ratios of CH_3I to satellite retrievals of PAR and surface ocean temperature, revealing a link to solar radiation (e.g. Happell et al., 1996; Yokouchi et al., 2001).

Although certain species of phytoplankton are capable of producing CH_3I (e.g. Manley and de la Cuesta 1997; Hughes et al., 2011), several studies also indicate a non-biological source for CH_3I in the surface ocean. This non-biological source, though not fully understood, requires light, a humic like substance at the surface ocean supplying a carbon source and methyl group, and reactive iodine (Moore and Zarifou 1994; Richter and Wallace 2004). Thus far, two chemical mechanisms have been proposed for the non-biological production of methyl iodide, one – a radical recombination of a methyl group and iodine involving UV photolysis (e.g. Moore and Zarifou 1994), and two, a substitution reaction involving the reduction of an oxidant, such as iron III (e.g. Williams et al. 2007).

3.4 Flux estimation

3.4.1 O_2-based emission estimates

We present a novel approach that facilitates a basin-wide halogenated VOC flux estimate using the robust relationship between airborne observations of O_2 and halogenated VOCs combined with modeled O_2 fluxes. Unlike the existing CAM-Chem halogenated VOC biogenic flux parameterization, this method does not rely on weekly retrievals of chl *a* at high latitudes, which are often patchy. In addition, our study indicates that $CHBr_3$, CH_2Br_2, and $CHClBr_2$ and CH_3I are better correlated with marine derived O_2 than the upstream influence of chl *a*.

For $CHBr_3$, CH_2Br_2, and $CHClBr_2$ we construct ocean emission inventories for January and February using a scaled version of gridded modeled air-sea O_2 fluxes and the slopes (i.e. molar ratios) of linear correlations between $\delta(O_2/N_2)$ and halogenated VOC mixing ratios (Fig. 10). O_2 fluxes were obtained from simulations using a configuration of the CESM model nudged to reanalysis temperatures and winds as described in Stephens et al. (2018). An earlier free running version of CESM was one of the best evaluated for reproducing the seasonal cycle of $\delta(O_2/N_2)$ over the Southern Ocean (Nevinson et al., 2015; 2016). To date, the north-south gradient in atmospheric O_2 has not been well reproduced by any models (Resplandy et al., 2016). Vertical gradients in O_2 on ORCAS indicate that CESM overestimated gradients by 47% on average; accordingly, O_2 fluxes were adjusted downward by 47% to better match the observations. This is obviously a very simple adjustment to the modeled fluxes, and the actual air-sea O_2 flux biases in CESM likely have a great deal of spatial and temporal heterogeneity. We calculated an uncertainty for the CESM flux using a second, independent estimate of O_2 fluxes based on dissolved O_2 measurements in surface seawater. The Garcia and Keeling (2001) climatology has much smoother temporal and spatial patterns than CESM flux estimates but also results in overestimated atmospheric O_2 spatial gradients. We calculate the relative uncertainty in O_2 flux as the ratio of the mean absolute difference between gridded Garcia and Keeling values (2001; also adjusted down by 51 % everywhere to better match ORCAS observations) to the CESM model flux estimates in Regions 1 and 2 (adjusted down by 47% everywhere). These disagreements were 7.3 % and 3.4 % for Regions 1 and 2, respectively. Based on the ratios of halogenated VOC to O_2 mixing ratios in bivariate least squares regressions and these adjusted O_2 fluxes, we estimate mean emissions of $CHBr_3$ and CH_2Br_2 in Region 1 and Region 2. Relative uncertainty in the slopes (i.e., the standard deviation of the slopes) from these regressions and the mean relative uncertainties in regional O_2 fluxes were added in quadrature to yield uncertainties in calculated halogenated VOC emission rates.

Figure 10 shows the mean emissions for Jan. and Feb. of $CHBr_3$, CH_2Br_2, and $CHClBr_2$ in Region 1 and Region 2. Mean regional emissions of $CHBr_3$ and CH_2Br_2 and $CHClBr_2$ are 91 ± 8, 31 ± 17, and 11 ± 4 pmol m^{-2} hr^{-1} in Region 1 and 329 ± 23, 69 ± 5, and 24 ± 5 pmol m^{-2} hr^{-1} in Region 2 (Table 1). The mean flux of CH_3I in Region 2 is 392 ± 32 (Table 1). Table 1 also lists the mean Jan. and Feb. CAM-Chem emissions from Region 1 and Region 2, as well as emissions from several other observational and modeling Antarctic polar studies. Our estimates fall within the range of these other studies, which span every month of the year and whose estimated fluxes range from negative (i.e. from the atmosphere into the ocean) to 3500 pmol m^{-2} hr^{-1} $CHBr_3$ in a coastal bay during its peak in primary production. CAM-Chem emissions for all species are

significantly lower than our observationally derived values in Region 1, with the exception of CH_3I. Conversely, CAM-Chem emissions are significantly higher than our estimated emissions in Region 2, with the exception of $CHClBr_2$ in Region 1, which remains underpredicted by the model (Table 1). We note that in Region 2, CAM-Chem fluxes of $CHBr_3$ and CH_2Br_2, although still significantly different, are more similar to our estimated fluxes.

3.4.2 STILT-based emission estimates

Similar to our O_2-based emission estimates, we used the relationship between surface influence functions and CH_3I mixing ratios (Fig. 9) to predict a flux field in Region 1 (Fig. 11). We used a multiple linear regression (± 1standard deviations; Equation 2), where Hs_1 and Hs_2 are the downward shortwave radiation and detrital absorption surface influence functions, respectively, with an intercept b = 0.19 ± 0.01, and influence coefficients a_1 = 3.7E-5 ± 1.3E-5, a_2 = 3.5± 0.74, and an interaction term with the coefficient a_3 = -5.2E-4 ± 1.5E-4 (Fig.9c). These regression coefficients and interaction term were used to estimate an average non-biological flux of CH_3I (Fig. 11; Table 1). This method could be used in place of the current Bell et al. (2002) climatology to update near weekly (~8 day) emissions of CH_3I in future versions of CAM-Chem. Our estimated mean CH_3I flux in Region 1 (35 ± 29 pmol m^{-2} hr^{-1}) is significantly lower than the current CAM-Chem estimated emissions (Table 1). As noted in Sect. 3.2, our observations of CH_3I are also much lower than the modeled mixing ratios. As discussed above, the strong correlations between CH_3I and O_2 in Region 2 also suggest a dominant biological source for this compound in this region. As a result, we have not used this relationship to parameterize a flux for CH_3I in Region 2 (see Sect. 3.1.2 and 3.4.1 for details). We note that although it would be possible to provide STILT-based emission estimates for other halogenated VOCs (e.g. $CHBr_3$ and CH_2Br_2), the correlations these compounds were less strong with surface influence functions than those with O_2/N_2.

4 Conclusions

Our work combined TOGA and AWAS halogenated VOC airborne observations from the ORCAS and ATom-2 campaigns, with coincident measurements of O_2 and CO_2, geophysical datasets and numerical models, including the global atmospheric chemistry model CAM-Chem, and the Lagrangian transport model, STILT. We evaluated model predictions, calculated molar enrichment ratios, inferred regional sources, and provided novel means of parameterizing ocean fluxes. We found that the Southern Ocean MBL is enriched in halogenated VOCs, but that these MBL enhancements are less pronounced at higher latitudes, i.e., poleward of 60° S (Region 1) than over the productive Patagonian shelf (Region 2).. Overall, our results indicated that the Southern Ocean is a moderate regional sources of $CHBr_3$, CH_2Br_2, and CH_3I, and a weak source of $CHClBr_2$ and $CHBrCl_2$ in January and February. Good model-measurement correlations were obtained between our observations and simulations from the Community Earth System Model (CESM) atmospheric component with chemistry (CAM-Chem) for $CHBr_3$, CH_2Br_2, CH_3I, and $CHClBr_2$ but all showed significant differences in model:measurement ratios. The

model:measurement comparison for CH_3Br was satisfactory and for $CHBrCl_2$ the low levels present precluded us from making a complete assessment.

$CHBr_3$ and CH_2Br_2 exhibited strong and robust correlations with each other and with O_2 and weaker but statistically significant correlations with the influence of chl *a*, which is a proxy for phytoplankton biomass. $CHClBr_2$ and $CHBr_3$ were well correlated with one another, particularly in Region 2. Together, these correlations suggested a biological source for these gases over the Southern Ocean. We found that CH_3I mixing ratios in Region 1 were best correlated with a non-biological surface influence function, although biogenic CH_3I emissions appear important in Region 2.

Our flux estimates based on the relationship of halogenated VOC mixing ratios to O_2 and remotely sensed parameters (for CH_3I) were compared with those derived from global models and ship-based studies (Table 1). Our emission estimates of $CHBr_3$, CH_2Br_2, and $CHClBr_2$ are significantly higher than CAM-Chem's globally prescribed emissions in Region 1, where halogenated VOC mixing ratios are under predicted (Table 1; Fig. 5). Similarly, our estimate of $CHClBr_2$ emissions is also significantly higher than CAM-Chem's in Region 2, where $CHClBr_2$ mixing ratios remained underpredicted. Yet, to the best of our knowledge, CAM-Chem's global parameterization of halogenated VOC fluxes has not been compared with data at high latitudes. Indeed, our emission estimates of $CHBr_3$, CH_2Br_2, CH_3I fall within a range of CAM-Chem's esimtates (on the low end) and most prior estimates based on either other models or localized studies using seawater-side measurements from the Antarctic polar region in summer (on the high end). In the case of CH_3I, our estimated emissions suggest that the prescribed emissions in CAM-Chem may be too high in Region 1 and Region 2. Our parameterizations of the CH_3I flux could be used to explore inter-annual variability in emissions, which is not captured by the Bell et al. (2002) CH_3I climatology currently employed in CAM-Chem.

To extend these relationships to year-round and global parameterizations for use in global climate models, they must be studied using airborne observations in other seasons and regions. These approaches may help parameterize emissions of new species that can be correlated with surface influence functions or the biological production of oxygen or may improve existing emissions, where persistent biases exist. Finally, future airborne observations of halogenated VOCs have the potential to further improve our understanding of air-sea flux rates and their drivers for these chemically and climatically important gases over the Southern Ocean.

Data Availability. The ORCAS and ATom-2 datasets are publically available at https://doi.org/10.5065/D6SB445X ; (www.eol.ucar.edu/field_projects/orcas) and https://doi.org/10.3334/ORNLDAAC/1581.

Author Contributions. EA is responsible for the bulk of the conceptualization, formal analysis, writing, review, and editing with contributions from all authors. BBS and ECA were instrumental in the investigation and supervision related to this manuscript. RSH contributed to the conceptualization, as well as the investigation and halogenated VOC data curation for this project. BBS, EJM, and RFK were responsible for the data curation of $\delta(O_2/N_2)$ data and contributed to formal analysis involving these data. MSHM along with EAK were responsible for STILT data curation and formal analysis, and the conceptualization and formal analysis of

SITLT-based geostatistical influence functions and flux estimates were also informed by these two. DK, along with ST, JFL and ASL were responsible for constructing CAM halogenated VOC emissions and conducting CAM runs. MCL was responsible for CESM simulations yielding O_2 fluxes and comparing this product alongside the Garcia and Keeling O_2 climatology in CAM. KMC and CM were responsible for the data curation of CO_2 observations. AJH contributed to the investigation for halogenated VOC data.

Acknowledgements. We would like to thank the ORCAS and ATom-2 science teams and the NCAR Research Aviation Facility and NASA DC-8 pilots, technicians and mechanics for their support during the field campaigns. In addition, we appreciate the NCAR EOL staff who have facilitated computing and data archival. In particular, we thank Tim Newberger for his help in supporting the NOAA Picarro CO_2 observations and Andrew Watt for his help in supporting the AO2 O_2 observations. This work was made possible by grants from NSF Polar Programs (1501993, 1501997, 1501292, 1502301, 1543457), NSF Atmospheric Chemistry Grants 1535364, 1623745, and 1623748 and NASA funding of the EVS2 Atmospheric Tomography (ATom) project, as well as the support of the NCAR Advanced Study Program (ASP) Postdoctoral Fellowship Program and computing support from Yellowstone, provided by NCAR's Computational and Information Systems Laboratory. The National Center for Atmospheric Research is sponsored by the National Science Foundation.

References

Abrahamsson, K., Lorén, A., Wulff, A. and Wängberg, S.-Å.: Air–sea exchange of halocarbons: the influence of diurnal and regional variations and distribution of pigments, Deep Sea Research Part II: Topical Studies in Oceanography, 51(22-24), 2789–2805, doi:10.1016/j.dsr2.2004.09.005, 2004a.

Abrahamsson, K., Bertilsson, S., Chierici, M., Fransson, A., Froneman, P. W., Lorén, A. and Pakhomov, E. A.: Variations of biochemical parameters along a transect in the Southern Ocean, with special emphasis on volatile halogenated organic compounds, Deep Sea Research Part II: Topical Studies in Oceanography, 51(22-24), 2745–2756, doi:10.1016/j.dsr2.2004.09.004, 2004b.

Abrahamsson, K., Granfors, A., Ahnoff, M., Cuevas, C. A. and Saiz-Lopez, A.: Organic bromine compounds produced in sea ice in Antarctic winter, Nature Communications, 9(1), doi:10.1038/s41467-018-07062-8, 2018.

Anav, A., Friedlingstein, P., Beer, C., Ciais, P., Harper, A., Jones, C., Murray-Tortarolo, G., Papale, D., Parazoo, N. C., Peylin, P., Piao, S., Sitch, S., Viovy, N., Wiltshire, A. and Zhao, M.: Spatiotemporal patterns of terrestrial gross primary production: A review: GPP Spatiotemporal Patterns, Reviews of Geophysics, 53(3), 785–818, doi:10.1002/2015RG000483, 2015.

Apel, E.: ORCAS Trace Organic Gas Analyzer (TOGA) VOC Data. Version 1.0, [online] Available from: https://data.eol.ucar.edu/dataset/490.018 (Accessed 29 January 2019), 2017.

Apel, E. C., Hornbrook, R. S., Hills, A. J., Blake, N. J., Barth, M. C., Weinheimer, A., Cantrell, C., Rutledge, S. A., Basarab, B., Crawford, J., Diskin, G., Homeyer, C. R., Campos, T., Flocke, F., Fried, A., Blake, D. R., Brune, W., Pollack, I., Peischl, J., Ryerson, T., Wennberg, P. O., Crounse, J. D., Wisthaler, A., Mikoviny, T., Huey, G., Heikes, B., O'Sullivan, D. and Riemer, D. D.: Upper tropospheric ozone production from lightning NO_x -impacted convection: Smoke ingestion case study from the DC3 campaign, Journal of Geophysical Research: Atmospheres, 120(6), 2505–2523, doi:10.1002/2014JD022121, 2015.

Atkinson, H. M., Huang, R.-J., Chance, R., Roscoe, H. K., Hughes, C., Davison, B., Schönhardt, A., Mahajan, A. S., Saiz-Lopez, A., Hoffmann, T. and Liss, P. S.: Iodine emissions from the sea ice of the Weddell Sea, Atmospheric Chemistry and Physics, 12(22), 11229–11244, doi:10.5194/acp-12-11229-2012, 2012.

Atlas, E.: ORCAS Advanced Whole Air Sampler (AWAS) Data. Version 1.0, [online] Available from: https://data.eol.ucar.edu/dataset/490.027 (Accessed 29 January 2019), 2017.

Ayers, G. P.: Comment on regression analysis of air quality data, Atmospheric Environment, 35(13), 2423–2425, doi:10.1016/S1352-2310(00)00527-6, 2001.

Bates, T. S.: Preface [to special section on First Aerosol Characterization Experiment (AGE 1)], Journal of Geophysical Research: Atmospheres, 104(D17), 21645–21647, doi:10.1029/1999JD900365, 1999.

Bell, N., Hsu, L., Jacob, D. J., Schultz, M. G., Blake, D. R., Butler, J. H., King, D. B., Lobert, J. M. and Maier-Reimer, E.: Methyl iodide: Atmospheric budget and use as a tracer of marine convection in global models: GLOBAL ATMOSPHERIC METHYL IODIDE, Journal of Geophysical Research: Atmospheres, 107(D17), ACH 8–1–ACH 8–12, doi:10.1029/2001JD001151, 2002.

Blake, N. J., Blake, D. R., Wingenter, O. W., Sive, B. C., Kang, C. H., Thornton, D. C., Bandy, A. R., Atlas, E., Flocke, F., Harris, J. M. and Rowland, F. S.: Aircraft measurements of the latitudinal, vertical, and seasonal variations of NMHCs, methyl nitrate, methyl halides, and DMS during the First Aerosol Characterization Experiment (ACE 1), Journal of Geophysical Research: Atmospheres, 104(D17), 21803–21817, doi:10.1029/1999JD900238, 1999.

Blei, E. and Heal, M. R.: Methyl bromide and methyl chloride fluxes from temperate forest litter, Atmospheric Environment, 45(8), 1543–1547, doi:10.1016/j.atmosenv.2010.12.044, 2011.

Bloss, W. J., J. D. Lee, G. P. Johnson, R. Sommariva, D. E. Heard, A. Saiz-Lopez, J. M. C. Plane, G. McFiggans, M. Flynn, P. Williams, A. R. Rickard and Z. L. Fleming: Impact of halogen monoxide chemistry upon boundary layer OH and HO_2 concentrations at a coastal site, Geophysical Research Letters, 32(6), doi:10.1029/2004GL022084, 2005.

Boden, T., Andres, R. and Marland, G.: Global, Regional, and National Fossil-Fuel CO_2 Emissions (1751 - 2014) (V. 2017), [online] Available from: https://www.osti.gov/servlets/purl/1389331/ (Accessed 25 November 2018), 2017.

Boucher, O., Moulin, C., Belviso, S., Aumont, O., Bopp, L., Cosme, E., von Kuhlmann, R., Lawrence, M. G., Pham, M., Reddy, M. S., Sciare, J. and Venkataraman, C.: DMS atmospheric concentrations and sulphate aerosol indirect radiative forcing: a sensitivity study to the DMS source representation and oxidation, Atmospheric Chemistry and Physics, 3(1), 49–65, doi:10.5194/acp-3-49-2003, 2003.

Butler, J. H., King, D. B., Lobert, J. M., Montzka, S. A., Yvon-Lewis, S. A., Hall, B. D., Warwick, N. J., Mondeel, D. J., Aydin, M. and Elkins, J. W.: Oceanic distributions and emissions of short-lived halocarbons: OCEANIC EMISSIONS OF SHORT-LIVED HALOCARBONS, Global Biogeochemical Cycles, 21(1), doi:10.1029/2006GB002732, 2007.

Cantrell, C. A.: Technical Note: Review of methods for linear least-squares fitting of data and application to atmospheric chemistry problems, Atmospheric Chemistry and Physics, 8(17), 5477–5487, doi:10.5194/acp-8-5477-2008, 2008.

Carpenter, L. J., Liss, P. S. and Penkett, S. A.: Marine organohalogens in the atmosphere over the Atlantic and Southern Oceans: MARINE ORGANOHALOGENS IN THE ATMOSPHERE, Journal of Geophysical Research: Atmospheres, 108(D9), n/a–n/a, doi:10.1029/2002JD002769, 2003.

Carpenter, L. J., Wevill, D. J., Palmer, C. J. and Michels, J.: Depth profiles of volatile iodine and bromine-containing halocarbons in coastal Antarctic waters, Marine Chemistry, 103(3-4), 227–236, doi:10.1016/j.marchem.2006.08.003, 2007.

Carpenter, L. J., Jones, C. E., Dunk, R. M., Hornsby, K. E. and Woeltjen, J.: Air-sea fluxes of biogenic bromine from the tropical and North Atlantic Ocean, Atmospheric Chemistry and Physics, 9(5), 1805–1816, doi:10.5194/acp-9-1805-2009, 2009.

Chuck, A. L.: Oceanic distributions and air-sea fluxes of biogenic halocarbons in the open ocean, Journal of Geophysical Research, 110(C10), doi:10.1029/2004JC002741, 2005.

Colomb, A., Yassaa, N., Williams, J., Peeken, I. and Lochte, K.: Screening volatile organic compounds (VOCs) emissions from five marine phytoplankton species by head space gas chromatography/mass spectrometry (HS-GC/MS), Journal of Environmental Monitoring, 10(3), 325, doi:10.1039/b715312k, 2008.

Drewer, J., Heal, K. V., Smith, K. A. and Heal, M. R.: Methyl bromide emissions to the atmosphere from temperate woodland ecosystems, Global Change Biology, doi:10.1111/j.1365-2486.2008.01676.x, 2008.

Emmons, L. K., Walters, S., Hess, P. G., Lamarque, J.-F., Pfister, G. G., Fillmore, D., Granier, C., Guenther, A., Kinnison, D., Laepple, T., Orlando, J., Tie, X., Tyndall, G., Wiedinmyer, C., Baughcum, S. L. and Kloster, S.: Description and evaluation of the Model for Ozone and Related chemical Tracers, version 4 (MOZART-4), Geoscientific Model Development, 3(1), 43–67, doi:10.5194/gmd-3-43-2010, 2010.

Fernandez, R. P., Salawitch, R. J., Kinnison, D. E., Lamarque, J.-F. and Saiz-Lopez, A.: Bromine partitioning in the tropical tropopause layer: implications for stratospheric injection, Atmospheric Chemistry and Physics, 14(24), 13391–13410, doi:10.5194/acp-14-13391-2014, 2014.

Finlayson-Pitts, B. J.: The Tropospheric Chemistry of Sea Salt: A Molecular-Level View of the Chemistry of NaCl and NaBr, Chemical Reviews, 103(12), 4801–4822, doi:10.1021/cr020653t, 2003.

Garcia, H. E. and Keeling, R. F.: On the global oxygen anomaly and air-sea flux, Journal of Geophysical Research: Oceans, 106(C12), 31155–31166, doi:10.1029/1999JC000200, 2001.

Gent, P. R., Danabasoglu, G., Donner, L. J., Holland, M. M., Hunke, E. C., Jayne, S. R., Lawrence, D. M., Neale, R. B., Rasch, P. J., Vertenstein, M., Worley, P. H., Yang, Z.-L. and Zhang, M.: The Community Climate System Model Version 4, Journal of Climate, 24(19), 4973–4991, doi:10.1175/2011JCLI4083.1, 2011.

von Glasow, R. and Crutzen, P. J.: Model study of multiphase DMS oxidation with a focus on halogens, Atmospheric Chemistry and Physics, 4(3), 589–608, doi:10.5194/acp-4-589-2004, 2004.

von Glasow, R., von Kuhlmann, R., Lawrence, M. G., Platt, U. and Crutzen, P. J.: Impact of reactive bromine chemistry in the troposphere, Atmospheric Chemistry and Physics, 4(11/12), 2481–2497, doi:10.5194/acp-4-2481-2004, 2004.

Glover, D. M., Jenkins, W. J. and Doney, S. C.: Modeling Methods for Marine Science, Cambridge University Press., 2011.

Guenther, A. B., Jiang, X., Heald, C. L., Sakulyanontvittaya, T., Duhl, T., Emmons, L. K. and Wang, X.: The Model of Emissions of Gases and Aerosols from Nature version 2.1 (MEGAN2.1): an extended and updated framework for modeling biogenic emissions, Geoscientific Model Development, 5(6), 1471–1492, doi:10.5194/gmd-5-1471-2012, 2012.

Happell, J. D., Wallace, D. W. R., Wills, K. D., Wilke, R. J. and Neill, C. C.: A purge-and-trap capillary column gas chromatographic method for the measurement of halocarbons in water and air. [online] Available from: http://www.osti.gov/servlets/purl/366493-84sOfy/webviewable/ (Accessed 26 July 2018), 1996.

Hossaini, R., Mantle, H., Chipperfield, M. P., Montzka, S. A., Hamer, P., Ziska, F., Quack, B., Krüger, K., Tegtmeier, S., Atlas, E., Sala, S., Engel, A., Bönisch, H., Keber, T., Oram, D., Mills, G., Ordóñez, C., Saiz-Lopez, A., Warwick, N., Liang, Q., Feng, W., Moore, F., Miller, B. R., Marécal, V., Richards, N. A. D., Dorf, M. and Pfeilsticker, K.: Evaluating global emission inventories of biogenic bromocarbons, Atmospheric Chemistry and Physics, 13(23), 11819–11838, doi:10.5194/acp-13-11819-2013, 2013.

Hughes, C., Chuck, A. L., Rossetti, H., Mann, P. J., Turner, S. M., Clarke, A., Chance, R. and Liss, P. S.: Seasonal cycle of seawater bromoform and dibromomethane concentrations in a coastal bay on the western Antarctic Peninsula: BROMOCARBON SEASONALITY ANTARCTICA, Global Biogeochemical Cycles, 23(2), n/a–n/a, doi:10.1029/2008GB003268, 2009.

Hughes, C., Johnson, M., Utting, R., Turner, S., Malin, G., Clarke, A. and Liss, P. S.: Microbial control of bromocarbon concentrations in coastal waters of the western Antarctic Peninsula, Marine Chemistry, 151, 35–46, doi:10.1016/j.marchem.2013.01.007, 2013.

Hurrell, J. W., Hack, J. J., Shea, D., Caron, J. M. and Rosinski, J.: A New Sea Surface Temperature and Sea Ice Boundary Dataset for the Community Atmosphere Model, Journal of Climate, 21(19), 5145–5153, doi:10.1175/2008JCLI2292.1, 2008.

Keeling, R. F., Manning, A. C., McEvoy, E. M. and Shertz, S. R.: Methods for measuring changes in atmospheric O_2 concentration and their application in southern hemisphere air, Journal of Geophysical Research: Atmospheres, 103(D3), 3381–3397, doi:10.1029/97JD02537, 1998.

Lai, S. C., Williams, J., Arnold, S. R., Atlas, E. L., Gebhardt, S. and Hoffmann, T.: Iodine containing species in the remote marine boundary layer: A link to oceanic phytoplankton: IODINE SPECIES AND PHYTOPLANKTON, Geophysical Research Letters, 38(20), n/a–n/a, doi:10.1029/2011GL049035, 2011.

Lamarque, J.-F.: Response of a coupled chemistry-climate model to changes in aerosol emissions: Global impact on the hydrological cycle and the tropospheric burdens of OH, ozone, and NO_x, Geophysical Research Letters, 32(16), doi:10.1029/2005GL023419, 2005.

Lamarque, J.-F., Emmons, L. K., Hess, P. G., Kinnison, D. E., Tilmes, S., Vitt, F., Heald, C. L., Holland, E. A., Lauritzen, P. H., Neu, J., Orlando, J. J., Rasch, P. J. and Tyndall, G. K.: CAM-chem: description and evaluation of interactive atmospheric chemistry in the Community Earth System Model, Geoscientific Model Development, 5(2), 369–411, doi:10.5194/gmd-5-369-2012, 2012.

Laturnus, F.: Volatile halocarbons released from Arctic macroalgae, Marine Chemistry, 55(3-4), 359–366, doi:10.1016/S0304-4203(97)89401-7, 1996.

Liang, Q., Atlas, E., Blake, D., Dorf, M., Pfeilsticker, K. and Schauffler, S.: Convective transport of very short lived bromocarbons to the stratosphere, Atmospheric Chemistry and Physics, 14(11), 5781–5792, doi:10.5194/acp-14-5781-2014, 2014.

Lin, J. C.: A near-field tool for simulating the upstream influence of atmospheric observations: The Stochastic Time-Inverted Lagrangian Transport (STILT) model, Journal of Geophysical Research, 108(D16), ACH 2–1–ACH 2–17, doi:10.1029/2002JD003161, 2003.

Liu, X., Easter, R. C., Ghan, S. J., Zaveri, R., Rasch, P., Shi, X., Lamarque, J.-F., Gettelman, A., Morrison, H., Vitt, F., Conley, A., Park, S., Neale, R., Hannay, C., Ekman, A. M. L., Hess, P., Mahowald, N., Collins, W., Iacono, M. J., Bretherton, C. S., Flanner, M. G. and Mitchell, D.: Toward a minimal representation of aerosols in climate models: description and evaluation in the Community Atmosphere Model CAM5, Geoscientific Model Development, 5(3), 709–739, doi:10.5194/gmd-5-709-2012, 2012.

Manley, S. L. and Dastoor, M. N.: Methyl iodide (CH3I) production by kelp and associated microbes, Marine Biology, 98(4), 477–482, doi:10.1007/BF00391538, 1988.

Maslanik, J.: Near-Real-Time DMSP SSM/I-SSMIS Daily Polar Gridded Sea Ice Concentrations, Version 1, 1999.

Mattson, E., Karlsson, A., Smith, W. O. and Abrahamsson, K.: The relationship between biophysical variables and halocarbon distributions in the waters of the Amundsen and Ross Seas, Antarctica, Marine Chemistry, 140-141, 1–9, doi:10.1016/j.marchem.2012.07.002, 2012.

Mattsson, E., Karlsson, A. and Abrahamsson, K.: Regional sinks of bromoform in the Southern Ocean: REGIONAL SINKS OF CHBR $_3$ IN THE ANTARCTIC, Geophysical Research Letters, 40(15), 3991–3996, doi:10.1002/grl.50783, 2013.

Moore, R. M. and Groszko, W.: Methyl iodide distribution in the ocean and fluxes to the atmosphere, Journal of Geophysical Research: Oceans, 104(C5), 11163–11171, doi:10.1029/1998JC900073, 1999.

Moore, R. M. and Zafiriou, O. C.: Photochemical production of methyl iodide in seawater, Journal of Geophysical Research, 99(D8), 16415, doi:10.1029/94JD00786, 1994.

Moore, R. M., Webb, M., Tokarczyk, R. and Wever, R.: Bromoperoxidase and iodoperoxidase enzymes and production of halogenated methanes in marine diatom cultures, Journal of Geophysical Research: Oceans, 101(C9), 20899–20908, doi:10.1029/96JC01248, 1996.

Murphy, D. M., Froyd, K. D., Bian, H., Brock, C. A., Dibb, J. E., DiGangi, J. P., Diskin, G., Dollner, M., Kupc, A., Scheuer, E. M., Schill, G. P., Weinzierl, B., Williamson, C. J. and Yu, P.: The distribution of sea-salt aerosol in the global troposphere, Atmospheric Chemistry and Physics Discussions, 1–27, doi:10.5194/acp-2018-1013, 2018.

NASA Goddard Space Flight Center, O. E. L.: SeaWiFS Ocean Color Data, 2014.

National Centers For Environmental Prediction/National Weather Service/NOAA/U.S. Department Of Commerce: NCEP GDAS/FNL 0.25 Degree Global Tropospheric Analyses and Forecast Grids, 2015.

Navarro, M. A., Atlas, E. L., Saiz-Lopez, A., Rodriguez-Lloveras, X., Kinnison, D. E., Lamarque, J.-F., Tilmes, S., Filus, M., Harris, N. R. P., Meneguz, E., Ashfold, M. J., Manning, A. J., Cuevas, C. A., Schauffler, S. M. and Donets, V.: Airborne measurements of organic bromine compounds in the Pacific tropical tropopause layer, Proceedings of the National Academy of Sciences, 112(45), 13789–13793, doi:10.1073/pnas.1511463112, 2015.

Neale, R. B., Richter, J., Park, S., Lauritzen, P. H., Vavrus, S. J., Rasch, P. J. and Zhang, M.: The Mean Climate of the Community Atmosphere Model (CAM4) in Forced SST and Fully Coupled Experiments, Journal of Climate, 26(14), 5150–5168, doi:10.1175/JCLI-D-12-00236.1, 2013.

Nevison, C. D., Manizza, M., Keeling, R. F., Kahru, M., Bopp, L., Dunne, J., Tiputra, J., Ilyina, T. and Mitchell, B. G.: Evaluating the ocean biogeochemical components of Earth system models using atmospheric potential oxygen and ocean color data, Biogeosciences, 12(1), 193–208, doi:10.5194/bg-12-193-2015, 2015.

Nevison, C. D., Manizza, M., Keeling, R. F., Stephens, B. B., Bent, J. D., Dunne, J., Ilyina, T., Long, M., Resplandy, L., Tjiputra, J. and Yukimoto, S.: Evaluating CMIP5 ocean biogeochemistry and Southern Ocean carbon

uptake using atmospheric potential oxygen: Present-day performance and future projection: CMIP5 APO AND SOUTHERN OCEAN CARBON FLUX, Geophysical Research Letters, 43(5), 2077–2085, doi:10.1002/2015GL067584, 2016.

Nightingale, P. D., Malin, G. and Liss, P. S.: Production of chloroform and other low molecular-weight halocarbons by some species of macroalgae, Limnology and Oceanography, 40(4), 680–689, doi:10.4319/lo.1995.40.4.0680, 1995.

Nightingale, P. D., Malin, G., Law, C. S., Watson, A. J., Liss, P. S., Liddicoat, M. I., Boutin, J. and Upstill-Goddard, R. C.: In situ evaluation of air-sea gas exchange parameterizations using novel conservative and volatile tracers, Global Biogeochemical Cycles, 14(1), 373–387, 2000.

Obrist, D., Tas, E., Peleg, M., Matveev, V., Faïn, X., Asaf, D. and Luria, M.: Bromine-induced oxidation of mercury in the mid-latitude atmosphere, Nature Geoscience, 4, 22, 2010.

Ordóñez, C., Lamarque, J.-F., Tilmes, S., Kinnison, D. E., Atlas, E. L., Blake, D. R., Sousa Santos, G., Brasseur, G. and Saiz-Lopez, A.: Bromine and iodine chemistry in a global chemistry-climate model: description and evaluation of very short-lived oceanic sources, Atmospheric Chemistry and Physics, 12(3), 1423–1447, doi:10.5194/acp-12-1423-2012, 2012.

Quack, B. and Wallace, D. W. R.: Air-sea flux of bromoform: Controls, rates, and implications: AIR-SEA FLUX OF BROMOFORM, Global Biogeochemical Cycles, 17(1), doi:10.1029/2002GB001890, 2003.

Raimund, S., Quack, B., Bozec, Y., Vernet, M., Rossi, V., Garçon, V., Morel, Y. and Morin, P.: Sources of short-lived bromocarbons in the Iberian upwelling system, Biogeosciences, 8(6), 1551–1564, doi:10.5194/bg-8-1551-2011, 2011.

Read, K. A., Mahajan, A. S., Carpenter, L. J., Evans, M. J., Faria, B. V. E., Heard, D. E., Hopkins, J. R., Lee, J. D., Moller, S. J., Lewis, A. C., Mendes, L., McQuaid, J. B., Oetjen, H., Saiz-Lopez, A., Pilling, M. J. and Plane, J. M. C.: Extensive halogen-mediated ozone destruction over the tropical Atlantic Ocean, Nature, 453(7199), 1232–1235, doi:10.1038/nature07035, 2008.

Resplandy, L., Keeling, R. F., Stephens, B. B., Bent, J. D., Jacobson, A., Rödenbeck, C. and Khatiwala, S.: Constraints on oceanic meridional heat transport from combined measurements of oxygen and carbon, Climate Dynamics, 47(9-10), 3335–3357, doi:10.1007/s00382-016-3029-3, 2016.

Reygondeau, G., Longhurst, A., Martinez, E., Beaugrand, G., Antoine, D. and Maury, O.: Dynamic biogeochemical provinces in the global ocean: DYNAMIC BIOGEOCHEMICAL PROVINCES, Global Biogeochemical Cycles, 27(4), 1046–1058, doi:10.1002/gbc.20089, 2013.

Richter, U. and Wallace, D. W. R.: Production of methyl iodide in the tropical Atlantic Ocean: PRODUCTION OF METHYL IODIDE, Geophysical Research Letters, 31(23), doi:10.1029/2004GL020779, 2004.

Rienecker, M. M., Suarez, M. J., Todling, R., Bacmeister, J., Takacs, L., Liu, H. C., Gu, W., Sienkiewicz, M., Koster, R. D., Gelaro, R., Stajner, I. and Nielsen, J. E.: The GEOS-5 Data Assimilation System – Documentation of Versions 5.0.1, 5.1.0, and 5.2.0, NASA/TM-2008-104606., 2008.

Saiz-Lopez, A., Mahajan, A. S., Salmon, R. A., Bauguitte, S. J.-B., Jones, A. E., Roscoe, H. K. and Plane, J. M. C.: Boundary Layer Halogens in Coastal Antarctica, Science, 317(5836), 348–351, doi:10.1126/science.1141408, 2007.

Saiz-Lopez, A., Lamarque, J.-F., Kinnison, D. E., Tilmes, S., Ordóñez, C., Orlando, J. J., Conley, A. J., Plane, J. M. C., Mahajan, A. S., Sousa Santos, G., Atlas, E. L., Blake, D. R., Sander, S. P., Schauffler, S., Thompson, A. M. and Brasseur, G.: Estimating the climate significance of halogen-driven ozone loss in the tropical marine troposphere, Atmospheric Chemistry and Physics, 12(9), 3939–3949, doi:10.5194/acp-12-3939-2012, 2012.

Saiz-Lopez, A., Fernandez, R. P., Ordóñez, C., Kinnison, D. E., Gómez Martín, J. C., Lamarque, J.-F. and Tilmes, S.: Iodine chemistry in the troposphere and its effect on ozone, Atmospheric Chemistry and Physics, 14(23), 13119–13143, doi:10.5194/acp-14-13119-2014, 2014.

Salawitch, R. J., Canty, T., Kurosu, T., Chance, K., Liang, Q., da Silva, A., Pawson, S., Nielsen, J. E., Rodriguez, J. M., Bhartia, P. K., Liu, X., Huey, L. G., Liao, J., Stickel, R. E., Tanner, D. J., Dibb, J. E., Simpson, W. R., Donohoue, D., Weinheimer, A., Flocke, F., Knapp, D., Montzka, D., Neuman, J. A., Nowak, J. B., Ryerson, T. B., Oltmans, S., Blake, D. R., Atlas, E. L., Kinnison, D. E., Tilmes, S., Pan, L. L., Hendrick, F., Van Roozendael, M., Kreher, K., Johnston, P. V., Gao, R. S., Johnson, B., Bui, T. P., Chen, G., Pierce, R. B., Crawford, J. H. and Jacob, D. J.: A new interpretation of total column BrO during Arctic spring: FRONTIER, Geophysical Research Letters, 37(21), n/a–n/a, doi:10.1029/2010GL043798, 2010.

Schauffler, S. M., Atlas, E. L., Blake, D. R., Flocke, F., Lueb, R. A., Lee-Taylor, J. M., Stroud, V. and Travnicek, W.: Distributions of brominated organic compounds in the troposphere and lower stratosphere, Journal of Geophysical Research: Atmospheres, 104(D17), 21513–21535, doi:10.1029/1999JD900197, 1999.

Schroeder, W. H., Anlauf, K. G., Barrie, L. A., Lu, J. Y., Steffen, A., Schneeberger, D. R. and Berg, T.: Arctic springtime depletion of mercury, Nature, 394, 331, 1998.

Simpson, W. R., Brown, S. S., Saiz-Lopez, A., Thornton, J. A. and von Glasow, R.: Tropospheric Halogen Chemistry: Sources, Cycling, and Impacts, Chemical Reviews, 115(10), 4035–4062, doi:10.1021/cr5006638, 2015.

Sive, B. C., Varner, R. K., Mao, H., Blake, D. R., Wingenter, O. W. and Talbot, R.: A large terrestrial source of methyl iodide, Geophysical Research Letters, 34(17), doi:10.1029/2007GL030528, 2007.

Stephens, B.: ORCAS Merge Products. Version 1.0, [online] Available from: https://data.eol.ucar.edu/dataset/490.024 (Accessed 31 December 2018), 2017.

Stephens, B. B., Keeling, R. F., Heimann, M., Six, K. D., Murnane, R. and Caldeira, K.: Testing global ocean carbon cycle models using measurements of atmospheric O_2 and CO_2 concentration, Global Biogeochemical Cycles, 12(2), 213–230, doi:10.1029/97GB03500, 1998.

Stephens, B. B., Keeling, R. F. and Paplawsky, W. J.: Shipboard measurements of atmospheric oxygen using a vacuum-ultraviolet absorption technique, Tellus B, 55(4), 857–878, doi:10.1046/j.1435-6935.2003.00075.x, 2003.

Stephens, B. B., Long, M. C., Keeling, R. F., Kort, E. A., Sweeney, C., Apel, E. C., Atlas, E. L., Beaton, S., Bent, J. D., Blake, N. J., Bresch, J. F., Casey, J., Daube, B. C., Diao, M., Diaz, E., Dierssen, H., Donets, V., Gao, B.-C., Gierach, M., Green, R., Haag, J., Hayman, M., Hills, A. J., Hoecker-Martínez, M. S., Honomichl, S. B., Hornbrook, R. S., Jensen, J. B., Li, R.-R., McCubbin, I., McKain, K., Morgan, E. J., Nolte, S., Powers, J. G., Rainwater, B., Randolph, K., Reeves, M., Schauffler, S. M., Smith, K., Smith, M., Stith, J., Stossmeister, G., Toohey, D. W. and Watt, A. S.: The O_2/N_2 Ratio and CO_2 Airborne Southern Ocean Study, Bulletin of the American Meteorological Society, 99(2), 381–402, doi:10.1175/BAMS-D-16-0206.1, 2018.

Sturges, W. T., Cota, G. F. and Buckley, P. T.: Bromoform emission from Arctic ice algae, Nature, 358, 660, 1992.

Sturges, W. T., Cota, G. F. and Buckley, P. T.: Vertical profiles of bromoform in snow, sea ice, and seawater in the Canadian Arctic, Journal of Geophysical Research: Oceans, 102(C11), 25073–25083, doi:10.1029/97JC01860, 1997.

Tilmes, S., Lamarque, J.-F., Emmons, L. K., Kinnison, D. E., Marsh, D., Garcia, R. R., Smith, A. K., Neely, R. R., Conley, A., Vitt, F., Val Martin, M., Tanimoto, H., Simpson, I., Blake, D. R. and Blake, N.: Representation of the Community Earth System Model (CESM1) CAM4-chem within the Chemistry-Climate Model Initiative (CCMI), Geoscientific Model Development, 9(5), 1853–1890, doi:10.5194/gmd-9-1853-2016, 2016.

Tohjima, Y.: Preparation of gravimetric standards for measurements of atmospheric oxygen and reevaluation of atmospheric oxygen concentration, Journal of Geophysical Research, 110(D11), doi:10.1029/2004JD005595, 2005.

Tokarczyk, R. and Moore, R. M.: Production of volatile organohalogens by phytoplankton cultures, Geophysical Research Letters, 21(4), 285–288, doi:10.1029/94GL00009, 1994.

Tortell, P. D. and Long, M. C.: Spatial and temporal variability of biogenic gases during the Southern Ocean spring bloom, Geophysical Research Letters, 36(1), doi:10.1029/2008GL035819, 2009.

Tortell, P. D., Asher, E. C., Ducklow, H. W., Goldman, J. A. L., Dacey, J. W. H., Grzymski, J. J., Young, J. N., Kranz, S. A., Bernard, K. S. and Morel, F. M. M.: Metabolic balance of coastal Antarctic waters revealed by autonomous $p\,CO_2$ and ΔO_2/Ar measurements: metabolic balence of Antarctic waters, Geophysical Research Letters, 41(19), 6803–6810, doi:10.1002/2014GL061266, 2014.

Williams, J., Gros, V., Atlas, E., Maciejczyk, K., Batsaikhan, A., Schöler, H. F., Forster, C., Quack, B., Yassaa, N., Sander, R. and Van Dingenen, R.: Possible evidence for a connection between methyl iodide emissions and Saharan dust, Journal of Geophysical Research, 112(D7), doi:10.1029/2005JD006702, 2007.

Engel, A., and M. Rigby (Lead Authors), Burkholder, J. B., Fernandez, R. P., Froidevaux, L., Hall, B. D., Hossaini, R., Saito, T., Vollmer, M. K. and B. Yao, Update on Ozone-Depleteing Substances (ODSs) and Other Gases of Interest to the Montreal Protocol, Chapter 1 in *Scientific Assessment of Ozone Depletion: 2018*, Global Ozone Research and Monitoring Project-Report No. 58, World Meteorological Organization, Geneva, Switzerland, 2018.

Wofsy, S. C.: HIAPER Pole-to-Pole Observations (HIPPO): fine-grained, global-scale measurements of climatically important atmospheric gases and aerosols, Philosophical Transactions of the Royal Society A: Mathematical, Physical and Engineering Sciences, 369(1943), 2073–2086, doi:10.1098/rsta.2010.0313, 2011.

Wofsy, S. C., Afshar, S., Allen, H. M., Apel, E., Asher, E. C., Barletta, B., Bent, J., Bian, H., Biggs, B. C., Blake, D. R., Blake, N., Bourgois, I., Brock, C. A., Brune, W. H., Budney, J. W., Bui, T. P., Butler, A., Campuzano-Jost, P., Chang, C. S., Chin, M., Commane, R., Correa, G., Crounse, J. D., Cullis, P. D., Daube, B. C., Day, D. A., Dean-Day, J. M., Dibb, J. E., Digangi, J. P., Diskin, G. S., Dollner, M., Elkins, J. W., Erdesz, F., Fiore, A. M., Flynn, C. M., Froyd, K., Gesler, D. W., Hall, S. R., Hanisco, T. F., Hannun, R. A., Hills, A. J., Hintsa, E. J., Hoffmann, A., Hornbrook, R. S., Huey, L. G., Hughes, S., Jimenez, J. L., Johnson, B. J., Katich, J. M., Keeling, R., Kim, M. J., Kupc, A., Lait, L. R., Lamarque, J.-F., Liu, H. B., McKain, K., Mclaughlin, R. J., Meinardi, S., Miller, D. O., Montzka, S. A., Moore, F. L., Morgan, E. J., Murphy, D. M., Murray, L. T., Nault, B. A., Neuman, J. A., Newman, P. A., Nicely, J. M., Pan, X., Paplawsky, W., Peischl, J., Prather, M. J., Price, D. J., Ray, E., Reeves, J. M., Richardson, M., Rollins, A. W., Rosenlof, K. H., Ryerson, T. B., Scheuer, E., Schill, G. P., Schroder, J. C., Schwarz, J. P., St.Clair, J. M., Steenrod, S. D., Stephens, B. B., Strode, S. A., Sweeney, C., Tanner, D., Teng, A. P., Thames, A. B., Thompson, C. R., Ullmann, K., Veres, P. R., Vizenor, N., Wagner, N. L., Watt, A., Weber, R., Weinzierl, B., et al.: ATom: Merged Atmospheric Chemistry, Trace Gases, and Aerosols, [online] Available from: https://daac.ornl.gov/cgi-bin/dsviewer.pl?ds_id=1581 (Accessed 31 December 2018), 2018.

Xiang, B., Miller, S. M., Kort, E. A., Santoni, G. W., Daube, B. C., Commane, R., Angevine, W. M., Ryerson, T. B., Trainer, M. K., Andrews, A. E., Nehrkorn, T., Tian, H. and Wofsy, S. C.: Nitrous oxide (N_2O) emissions from California based on 2010 CalNex airborne measurements: California N_2O emissions, Journal of Geophysical Research: Atmospheres, 118(7), 2809–2820, doi:10.1002/jgrd.50189, 2013.

Yang, B., Yang, G.-P., Lu, X.-L., Li, L. and He, Z.: Distributions and sources of volatile chlorocarbons and bromocarbons in the Yellow Sea and East China Sea, Marine Pollution Bulletin, 95(1), 491–502, doi:10.1016/j.marpolbul.2015.03.009, 2015.

Yokouchi, Y., Nojiri, Y., Barrie, L. A., Toom-Sauntry, D. and Fujinuma, Y.: Atmospheric methyl iodide: High correlation with surface seawater temperature and its implications on the sea-to-air flux, Journal of Geophysical Research: Atmospheres, 106(D12), 12661–12668, doi:10.1029/2001JD900083, 2001.

Yokouchi, Y., Hasebe, F., Fujiwara, M., Takashima, H., Shiotani, M., Nishi, N., Kanaya, Y., Hashimoto, S., Fraser, P., Toom-Sauntry, D., Mukai, H. and Nojiri, Y.: Correlations and emission ratios among bromoform, dibromochloromethane, and dibromomethane in the atmosphere, Journal of Geophysical Research, 110(D23), doi:10.1029/2005JD006303, 2005.

Ziska, F., Quack, B., Abrahamsson, K., Archer, S. D., Atlas, E., Bell, T., Butler, J. H., Carpenter, L. J., Jones, C. E., Harris, N. R. P., Hepach, H., Heumann, K. G., Hughes, C., Kuss, J., Krüger, K., Liss, P., Moore, R. M., Orlikowska, A., Raimund, S., Reeves, C. E., Reifenhäuser, W., Robinson, A. D., Schall, C., Tanhua, T., Tegtmeier, S., Turner, S., Wang, L., Wallace, D., Williams, J., Yamamoto, H., Yvon-Lewis, S. and Yokouchi, Y.: Global sea-to-air flux climatology for bromoform, dibromomethane and methyl iodide, Atmospheric Chemistry and Physics, 13(17), 8915–8934, doi:10.5194/acp-13-8915-2013, 2013.

997 **Tables**

998 Table 1. Mean ± uncertainty (see Sect. 3.4.1 and 3.4.2 for details) halogenated VOC emission
999 estimates (pmol m^{-2} hr^{-1}) in Region 1 and Region 2 calculated in this study (with method
1000 indicated below each value), from CAM-Chem (Ordoñez et al., 2012) and from several other
1001 modeling and ship-based observational studies.

1002

Region/Months	**$CHBr_3$**	**CH_2Br_2**	**CH_3I**	**$CHClBr_2$**	**Reference**
Region 1 (JF) < 60° S	91 ± 8 O_2 Regr.	31 ± 18 O_2 Regr.	35 ± 29 MLR	11 ± 4 O_2 Regr.	This Study
Region 2 (JF) >55° S and <40° S	329 ± 23 O_2 Regr.	69 ± 5 O_2 Regr.	392 ±32 O_2 Regr.	25 ± 5 O_2 Regr.	This Study
Region 1 (JF)	10	1.9	120	0.38	CAM-Chem
Region 2 (JF)	360	44	800	8.7	CAM-Chem
Southern Ocean (≥50°S), (DJ)	200	200	200	----------	Ziska et al. 2013 (model)
Marguerite Bay (DJF)	3500	875	----------	----------	Hughes et al. 2009 (obs)
70°S-72°S Antarctica	1300	----------	----------	----------	Carpenter et al. 2007 (obs)
Southern Ocean (≥50°S) (Feb. - April)	225	312	708	----------	Butler et al. 2007 (obs)
40°S-52°S S. Atlantic (Sept.-Feb.)	-1670	----------	250	----------	Chuck et al. 2005
Southern Ocean (≥50°S), (DJ)	-330	----------	----------	----------	Mattson et al. 2013 (model)

1003

1004

1005

Figures

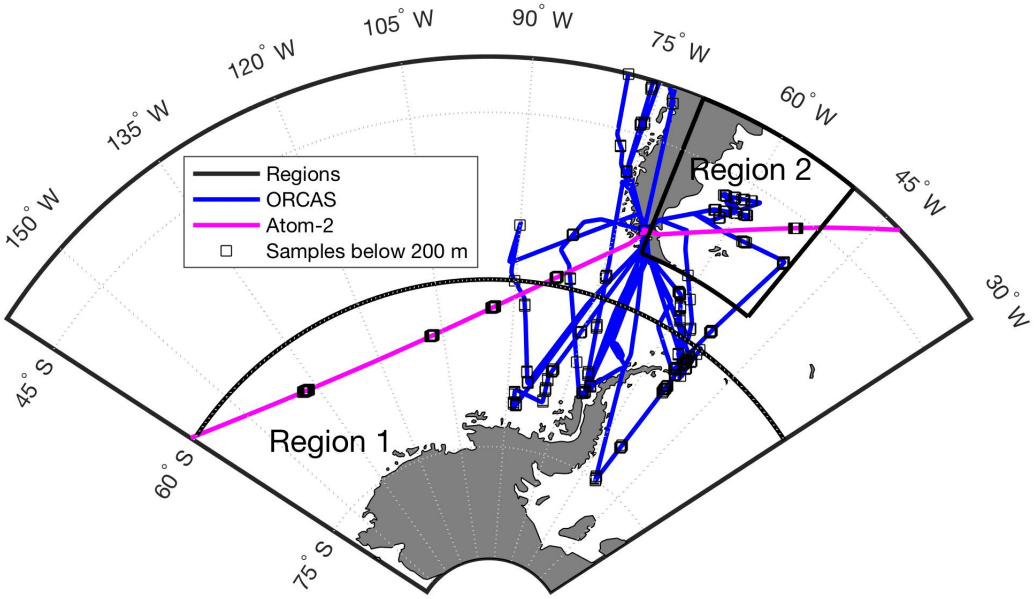

Figure 1. Overview map ORCAS and ATom-2 flight tracks in the study regions: 1) high latitudes in the Southern Hemisphere poleward 60° S and 2) the Patagonian Shelf. The ORCAS and ATom-2 aircraft flights and dips below 200 m that took place within these regions are also shown.

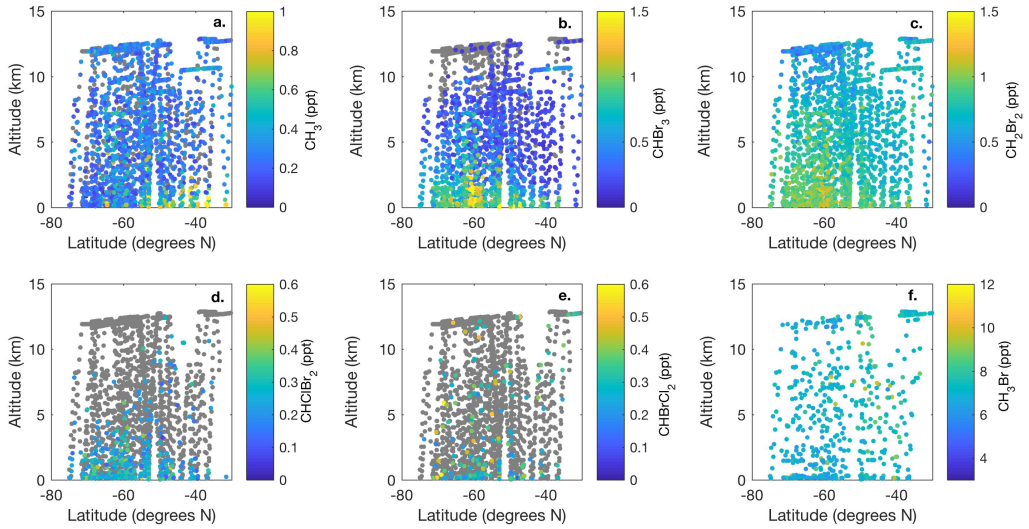

Figure 2. Meridional-altitudinal cross-sections of mixing ratios of a) CH_3I , b) $CHBr_3$, c) CH_2Br_2, d) $CHClBr_2$, and e) $CHBrCl_2$ from the TOGA and mixing ratios of f) CH_3Br from AWAS and WAS in 2016 and 2017, respectively, during the ORCAS and ATom-2 campaigns over the Southern Ocean in the austral summer. Note the different color bar scales. Gray points denote measurements below the detection limit of each species (CH_3I - 0.03 ppt, $CHBr_3$ – 0.2 ppt, CH_2Br_2 – 0.03 ppt, $CHClBr_2$ – 0.03 ppt, $CHBrCl_2$ – 0.05 ppt, CH_3Br – 0.2 ppt).

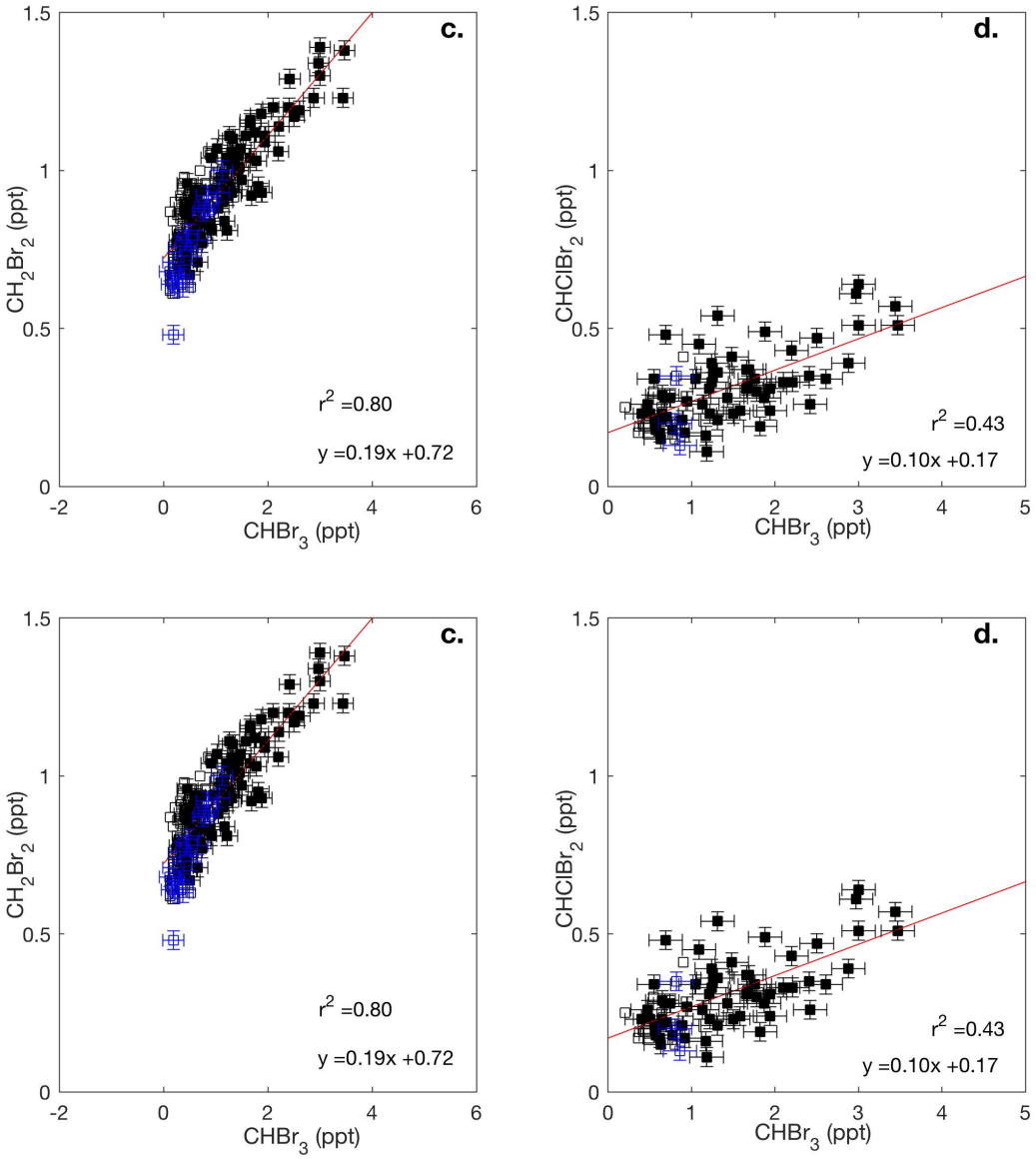

c.
d.
CH_2Br_2 (ppt)
$CHClBr_2$ (ppt)
$CHBr_3$ (ppt)
r^2 =0.80
y =0.19x +0.72
r^2 =0.43
y =0.10x +0.17

Figure 3. Mixing ratios of $CHBr_3$ vs. CH_2Br_2 and $CHClBr_2$ across the ORCAS and ATom-2 campaigns in Region 1 (Fig.3a,b) and in (Fig.3c,d), respectively. Type II major axis regression model (bivariate least squares regressions) are based on ORCAS data below 2 km and illustrate regional enhancement ratios. Error bars represent the uncertainty in halogenated VOC measurements.

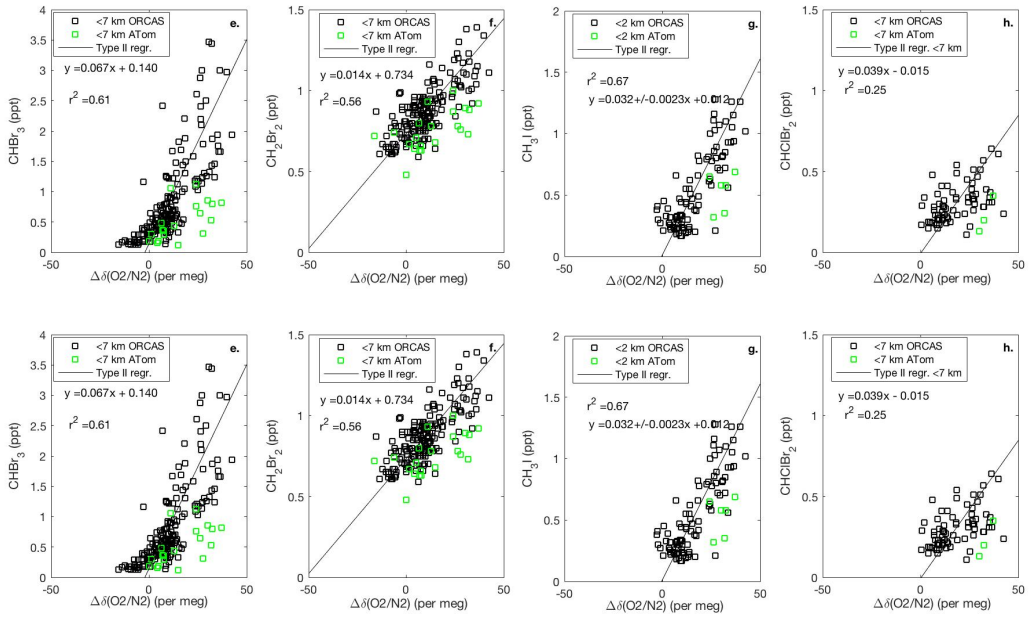

Figure 4. Mixing ratios of $CHBr_3$, CH_2Br_2, and CH_3I vs. O_2 on ORCAS and ATom-2 in Region 1, poleward of 60° S (a-d) and Region 2 over the Patagonian Shelf (e-h). Slopes ± standard errors from type II major axis regression model (bivariate least squares regression) fits of ORCAS data for regressions with $r^2 > 0.2$ (fits were calculated on variables scaled to their full range). The slopes reported in the figure are converted to pmol:mol ratios prior to estimating biogenic halogenated VOC fluxes based on modeled CESM O_2 fluxes. Data from above 7 km were excluded due to the influence of air masses transported from further north.

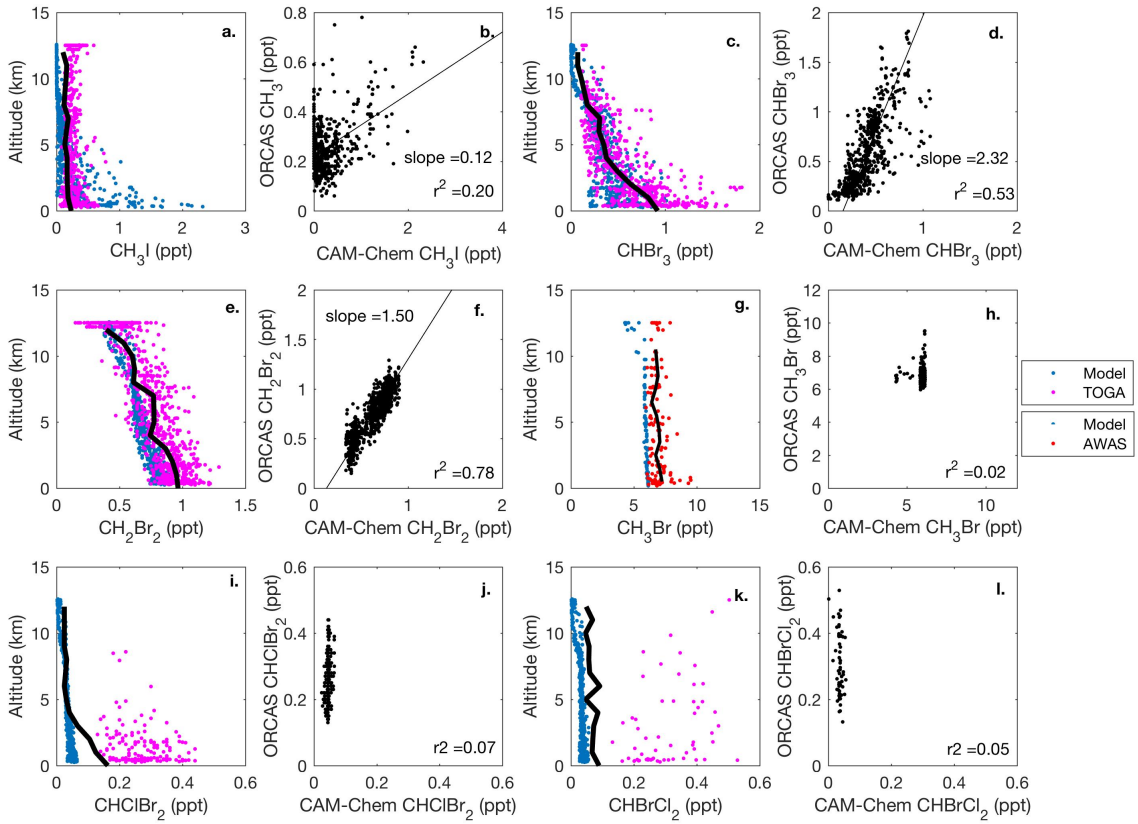

Fig 5. CAM-Chem1.2 model-aircraft measurement comparison during the ORCAS campaign between 1-12 km in Region 1, high latitudes in the Southern Hemisphere poleward 60° S. All regressions are type II major axis regression models bivariate least squares regressions (slopes are shown when the $r^2 \geq 0.2$). The bold, black line in each vertical profile represents the binned (mean) mixing ratio of halogenated VOC measurements at that altitude. The binned mean includes measurements below the detection limit (DL), which for this calculation are assigned a value equal to the DL multiplied by the percentage of data below detection. Modeled values include locations where observations were below the DL.

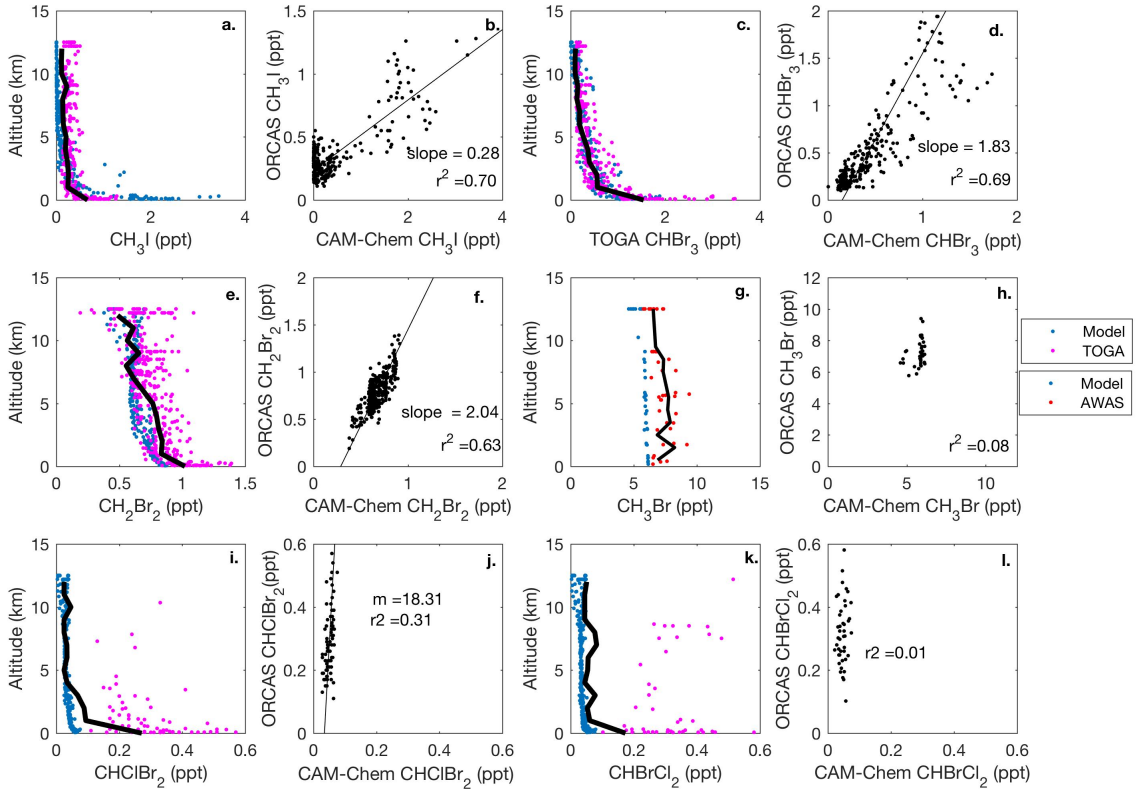

Figure 6. CAM-Chem 1.2 model-aircraft measurement (TOGA and AWAS) comparison during ORCAS campaign between 1-12 km in Region 2, the Patagonian Shelf. All regressions are type II major axis regression models bivariate least squares regressions (slopes are shown when the r^2 ≥ 0.2). The bold, black line in each vertical profile represents the binned (mean) mixing ratio of halogenated VOC measurements at that altitude. Again, the binned mean includes measurements below the detection limit (DL), which for this calculation are assigned a value equal to the DL multiplied by the percentage of data below detection. Modeled values include locations where observations were below the DL.

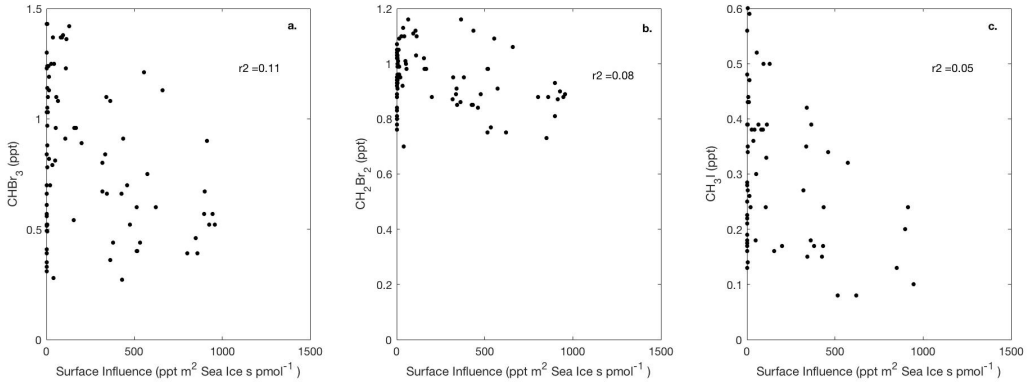

Figure 7. Linear type II regressions between influence functions convolved with sea ice distributions, which exclude land ice, and mixing ratios for $CHBr_3$, CH_2Br_2, and CH_3I in Region 1, poleward of 60° S. Surface influence (ppt m^2 s $pmol^{-1}$) in each grid cell was multiplied by fractional sea ice concentration surface field, which is unit-less, yielding sea ice surface influence function units of ppt m^2 s $pmol^{-1}$, as shown on the x-axis. Linear regression lines are not shown, as $p \geq 0.001$.

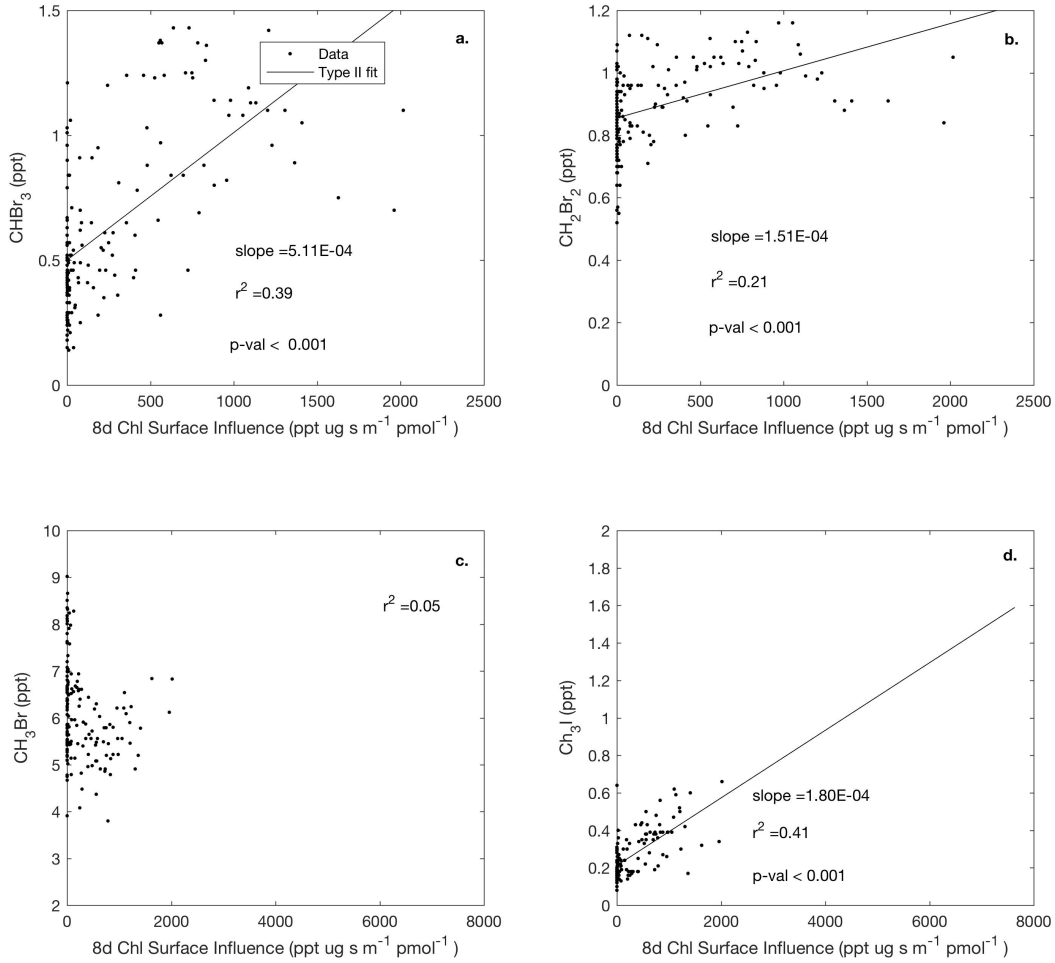

Figure 8. Linear type II regressions between influence functions of eight day composites of chl *a* and mixing ratios of halogenated VOCs (a-d) poleward of 60° S (Region 1). Surface influence (ppt m^2 s $pmol^{-1}$) in each grid cell was multiplied by the chl *a* (µg m^{-3}) surface field, resulting in surface influence function units of µg ppt s $pmol^{-1}$ m^{-1}, shown on the x-axis. Linear regression lines are shown where when $p < 0.001$.

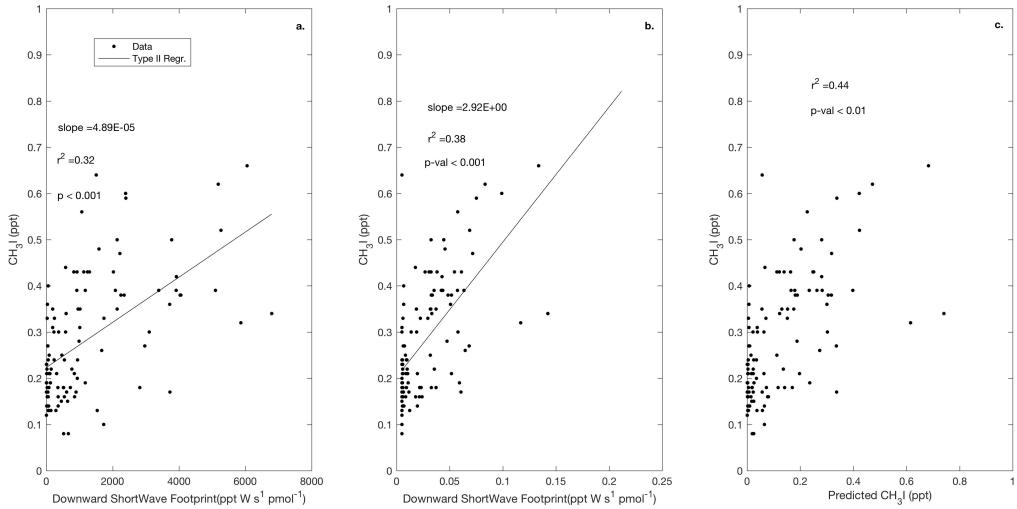

Figure 9. Observed CH_3I plotted against the surface influence functions of downward shortwave radiation (a) and absorption due to detritus (b). Predicted mixing ratios of CH_3I based on a multiple linear regressions (MLR) using these two predictors in Region 1 are shown in Fig. 9c according to Equation 3. Surface influence (ppt m^2 s $pmol^{-1}$) in each grid cell was multiplied by the surface source field, such as shortwave radiation at the surface (W m^{-2}), yielding units of ppt Ws $pmol^{-1}$, and the surface ocean's detrital absorption (m^{-1}), yielding units of ppt m s $pmol^{-1}$, shown on the x-axes.

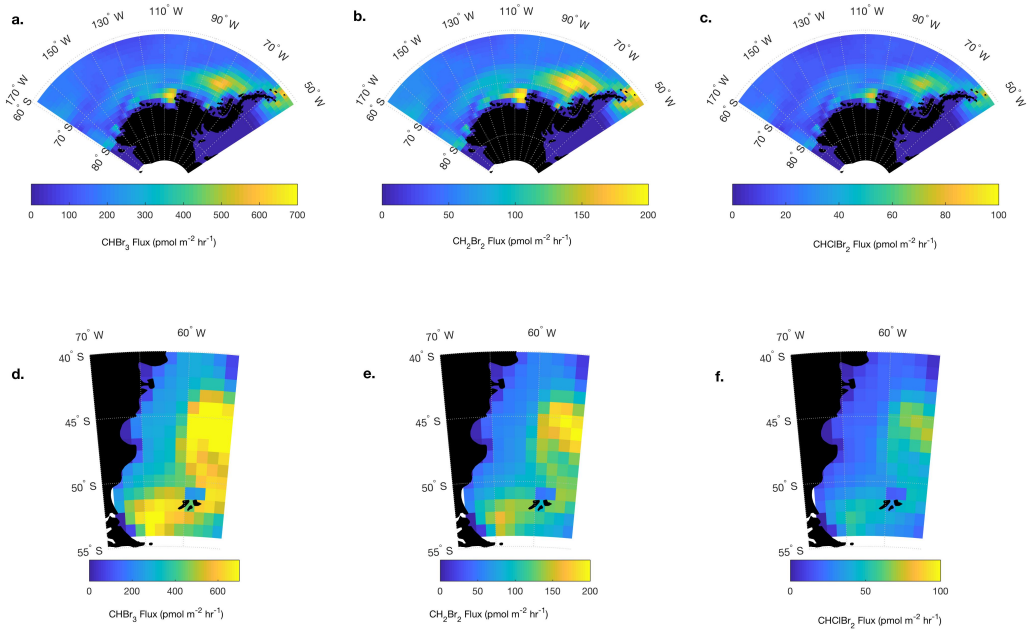

Figure 10. Resulting mean Jan. – Feb. 2016 O_2-based (parameterized) $CHBr_3$ and CH_2Br_2 and $CHClBr_2$ fluxes (pmol m^{-2} s^{-1}) in Region 1 (a-c) poleward of 60° S and Region 2 (d-f) over the Patagonian Shelf. CESM modeled O_2 fluxes are scaled by the slope between the oceanic contribution to $\delta(O_2/N_2)$ and $CHBr_3$ and CH_2Br_2, and $CHClBr_2$ reported in Fig. 4. Note that these fluxes represent mean estimated biogenic fluxes in Jan. -Feb. 2016 (see Sect. 3.4.1 for details).

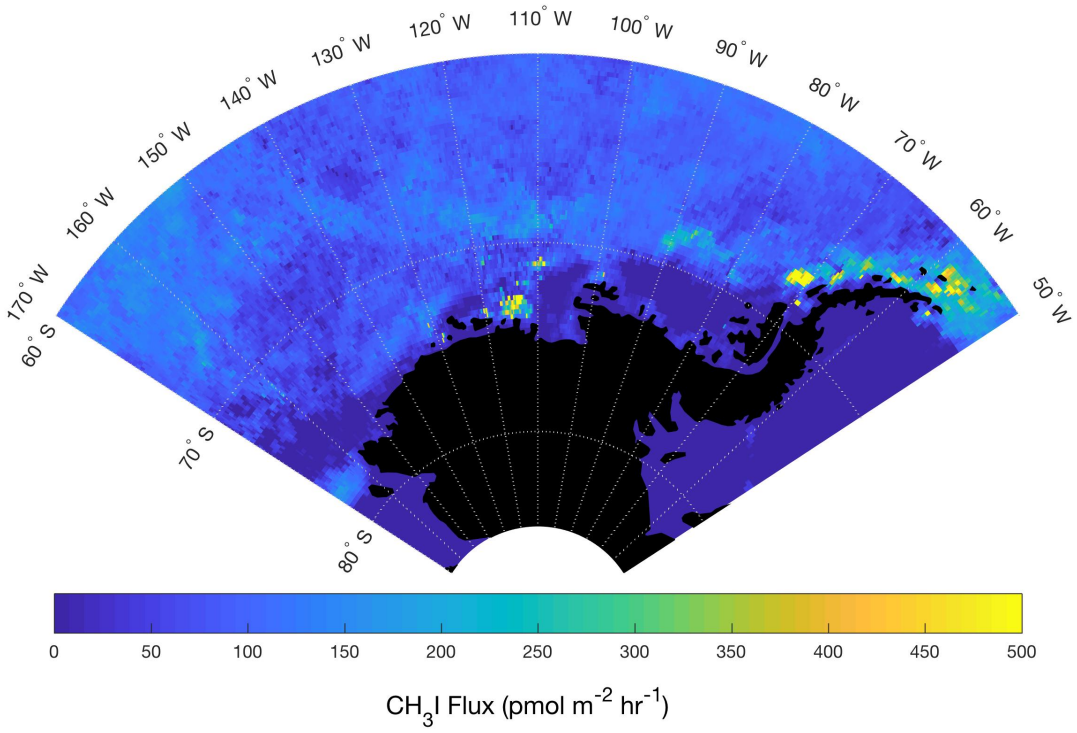

Figure 11. Mean estimated CH_3I fluxes for Jan. – Feb. The multilinear regression in Fig. 9 between CH_3I mixing ratios and geophysical influence functions related to shortwave radiation and detrital material at the sea surface was used to derive a mean flux field in Jan.-Feb., 2016 for Region 1.